Energy, Volume 360, September 2026, Article number 141560
DOI: 10.1016/j.energy.2026.141560

Eco-Cruising Control Under Cut-In Maneuvers Using Spatiotemporal Attention-Based Trajectory Prediction

Jie Li[1], Shengrong Li[1], Yuhang Lan[1], Abbas Fotouhi[2], Yonggang Liu[3*] and Zhen Chen[4*]

[1] Guangxi Key Lab of Manufacturing System and Advanced Manufacturing Technology, School of Mechanical Engineering, Guangxi University, Nanning 530003, China
[2] Advanced Vehicle Engineering Centre, School of Aerospace, Transport and Manufacturing, Cranfield University, Cranfield, Bedfordshire, MK43 0AL, UK
[3] State Key Laboratory of Mechanical Transmission for Advanced Equipment, College of Mechanical and Vehicle Engineering, Chongqing University 400044, Chongqing, China
[4]Faculty of Transportation Engineering, Kunming University of Science and Technology 650500, Kunming, China
Correspondence: Yonggang Liu (andyliuyg@cqu.edu.cn), Zheng Chen (chen@kust.edu.cn)

Abstract: With the rapid advancement of connected and automated vehicles technologies, eco-cruising control strategies have attracted increasing attention due to the significant potential for energy conservation. However, stochastic disturbances induced by human-driven vehicles (HDVs) can markedly compromise both energy efficiency and driving comfort. To tackle this challenge, a spatiotemporal prediction-based eco-cruising strategy is proposed to optimize velocity profiles by considering the spatiotemporal interaction among surrounding vehicles in a hierarchical framework. In the upper layer, a graph-based attention model is developed to capture spatiotemporal features from historical HDV trajectories, thereby accurately predicting their motion trajectories in mixed traffic environments. In the lower layer, a model predictive control integrated with a quadratic programming algorithm is designed to achieve ecological speed optimization accounting for random cut-in behaviors. Real world motion data are leveraged to validate the proposed approach, demonstrating that the proposed prediction model can accurately predict vehicle lane-change trajectories, while the overall performance is significantly improved under random cut-in maneuvers. Specifically, the proposed method achieves an average improvement of 16.23% in energy efficiency while ensuring preferable travel efficiency and driving comfort.

Key Words: electric vehicle, eco-cruising, energy efficiency, trajectory prediction, quadratic programming

I. INTRODUCTION

Transportation electrification has been widely acknowledged due to the influence of energy shortage and

Published by Elsevier. This is the Author Accepted Manuscript issued with: Creative Commons Attribution License (CC:BY 4.0).
The final published version (version of record) is available online at DOI:10.1016/j.energy.2026.141560. Please refer to any applicable publisher terms of use.

environment friendly [1]. Electric vehicles (EVs), plug-in hybrid electric vehicles (PHEVs) and hybrid electric vehicles (HEVs) have grown steadily in the past decade [2]. Among these new energy vehicles, EVs in particular, account for significant proportion in transportation electrification due to their superior performance in energy efficiency and driving comfort [3]. Additionally, with the advancement of connected and automated vehicles (CAVs) technologies, CAVs can obtain various types of driving environment information through sensors and vehicle-to-everything communication technologies [4, 5]. This capability allows CAVs to avoid abrupt braking, rapid acceleration, and unnecessary idling, while automatically planning velocity profiles to enhance driving safety and driving comfort [6]. Except for driving safety, energy efficiency has become a major concern with the emergence of electric connected and automated vehicles (ECAVs). Optimizing driving behaviors can significantly reduce energy consumption, and such strategies are commonly referred to as eco-driving [7]. These techniques typically optimize driving speed or lane-change behaviors considering driving conditions while satisfying complex constraints related to vehicle dynamics, driving safety, and driving comfort, with the objective of improving energy efficiency.

Extensive research has been conducted on various aspects of eco-driving to enhance energy efficiency by considering factors such as powertrain characteristics, road conditions, and signal phase and timing. Powertrain characteristic have a significant impact on ecological velocity and are therefore normally incorporated into speed optimization framework. P. Liao *et al.* [8] improved the state of charge (SOC) estimation accuracy by incorporating battery thermal effects into a powertrain-based longitudinal vehicle dynamics model for ECAVs, and subsequently employed dynamic programming (DP) to derive the optimal velocity profile. S. Wang *et al*. [9] estimated the powertrain energy consumption of HEVs using a pre-designed energy management system tailored to different driving scenarios, thereby optimizing the accurate ecological speed. In addition, road conditions play a significant role in determining feasible driving speed, and some studies have performed ecological velocity optimization by accounting for various road conditions including road gradient, curvature, and speed limits. H. Lee *et al*. [10] proposed an eco-driving strategy using reinforcement learning that explicitly incorporates factors road gradient and speed limits. Y. Wu *et al*. [11] addressed the eco-driving optimization problem under varying road gradients by integrating DP and proximal policy optimization (PPO) reinforcement learning, enabling online ecological velocity planning and achieving notable energy savings. S. R. Deshpande *et al*. [12] integrated an equivalent consumption

minimization strategy with DP for PHEVs ecological speed optimization, considering road speed limits and terrain. The aforementioned studies focus primarily on road information, whereas in urban driving scenarios, traffic lights exert a significant influence on eco-driving strategies. Z. Lei *et al*. [13] proposed an ecological speed optimization method that takes into account both traffic light phasing and timing as well as road data, employing the shortest path faster algorithm to enhance vehicle energy economy. T. Jayson *et al*. [14] applied Pontryagin's minimum principle to optimize ecological velocity of EVs in different urban traffic scenarios with signalized intersections, considering road gradient and regenerative braking to minimize the energy consumption. C. Wang *et al.* [15] utilized model predictive control (MPC) to optimize vehicle speed trajectories across multiple signalized intersections and employed an input convex neural network for real-time speed tracking, thereby enhancing overall energy efficiency. K. Lu *et al*. [16] utilized DP for ecological velocity planning at signalized intersections, followed by MPC for ecological speed trajectory tracking, thereby enabling smooth and uninterrupted driving to improve energy efficiency. Z. Zhu *et al.* [17] proposed a DRL-based eco-driving strategy with low onboard computational resources, enabling rapid optimization of the ego vehicle's speed based on traffic light information. However, these approaches plan the velocity of CAVs solely based on slowly varying road traffic information, whereas in real-world traffic environments, stochastic disturbances induced by human-driven vehicles (HDVs) can significantly affect the energy consumption of CAVs.

As illustrated in Fig. 1, disturbances imposed by surrounding HDVs on the CAV mainly manifest in two forms. Longitudinal stochastic disturbances, originating from the speed variations of the preceding vehicle, lead to frequent yet relatively mild speed fluctuations of the ego vehicle. In contrast, lateral disturbances induced by cut-in maneuvers of surrounding vehicles usually cause abrupt changes in inter-vehicle spacing, resulting in sharp and pronounced speed variations of the ego vehicle. Accordingly, substantial research have explored eco-driving under stochastic disturbances from surrounding vehicles [18, 19], while most studies primarily focus on longitudinal stochastic disturbances induced by preceding HDVs [20, 21]. J. Li *et al*. [22] proposed a multi-objective composite reward function that incorporates traffic factors, including stochastic disturbances from preceding HDVs, traffic signals and speed limits, and employed deep reinforcement learning to implement eco-driving control for HEVs. T. Ard *et al*. [23] designed an optimal speed planning method for passing through signalized intersections in mixed traffic environment. In this work, MPC is employed to avoid collisions with preceding vehicles, thereby improving

both energy efficiency and driving safety. J. Li *et al*. [24] generated dynamic updated traffic light information based on a queue-based traffic model and preceding vehicle information, and achieved speed optimization using deep deterministic policy gradient. K. Lu *et al*. [25] addressed uncertainties from HDVs in mixed traffic environments by integrating reinforcement learning and MPC to optimize the energy efficiency and driving safety of CAVs, respectively. B. Li *et al*. [26] optimized the ecological velocity based on global road information and applied rolling-horizon optimization control to handle the longitudinal stochastic behavior of preceding HDVs. To address lateral uncertainties caused by lane-change maneuvers of HDVs, some studies simplify and model lateral disturbances as equivalent longitudinal stochastic disturbances. Y. Hu *et al*. [27] modeled both HDV cut-in maneuvers and stochastic disturbances from the preceding vehicle as longitudinal disturbances, implementing a rolling-horizon approach to achieve eco-driving at signalized intersections. Y. Wang *et al*. [28] represented stochastic lane-change maneuvers as equivalent longitudinal disturbances to solve the eco-cruising optimal control problem (OCP) and explored the influence of cut-in behaviors on vehicles with heterogeneous powertrains. However, the aforementioned studies generally adopt passive methods to handle lateral stochastic disturbances caused by HDV cut-in maneuvers. Such approaches usually lead to pronounced velocity fluctuations in CAVs, consequently degrading both energy efficiency and driving comfort.

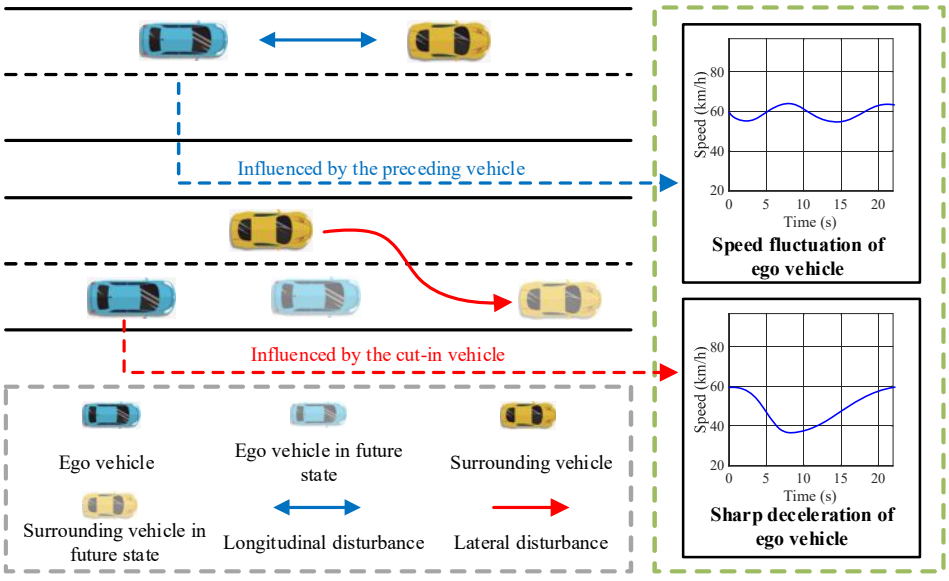


Fig. 1. The stochastic disturbances from surrounding vehicles.

To further mitigate stochastic disturbances from HDVs, recent studies have incorporated the lane-change prediction into the motion control of CAVs. In mixed traffic environments, anticipating HDV lane-change

maneuvers enables CAVs to presciently plan ecological velocity, enhancing both energy efficiency and driving comfort. X. Wang *et al*. [29] employed an attention mechanism to fuse sequential features extracted by an long short-term memory LSTM with vehicle interaction features from high definition maps, while also considering the road's geographic structure to enhance prediction accuracy. H. Sadid *et al*. [30] enhanced lane-change prediction accuracy by jointly modeling spatial interactions among HDVs and temporal dependencies in trajectory sequences using graph convolutional networks (GCNs) and temporal convolutional networks. D. Li *et al*. [31] proposed a hierarchical framework that decouples the trajectory prediction task into lateral and longitudinal components based on driving intentions and selecting path, and subsequently integrates both dimensions to predict the trajectories of HDVs. G. Chen *et al*. [32] developed an LSTM-based trajectory prediction model with an attention mechanism to capture interactions among HDVs, while incorporating driving styles to enhance lane-change trajectory forecasting. However, most previous studies primarily focus improving driving comfort and safety using lane-change predictions, while the energy efficiency is normally neglected. Recently, few studies have attempted to leverage lane-change prediction to enhance both energy efficiency and driving comfort. C. R. He *et al*. [33] employed a leader-follower game to capture the interaction between the ego vehicle and lane-changing vehicles, while MPC is applied to plan ecological velocity to improve energy efficiency. S. He *et al*. [34] utilized an unscented Kalman filter with the Payne–Whitham model to estimate traffic variations induced by HDV lane-change maneuvers, enabling adaptive ecological velocity optimization. Y. Liang *et al*. [35] applied a Bayesian network to predict the lane-change trajectory and employed quadratic programming (QP) to optimize the velocity of the CAV, thereby enhancing energy efficiency and driving comfort. However, existing prediction models typically fail to simultaneously capture both HDV interactions and temporal dependencies in motion sequences. The limitations in lane-change prediction can result in inaccurate estimations of inter-vehicle distance and cut-in timing, leading to suboptimal speed planning and degraded overall performance.

To enhance the overall performance of eco-cruising under random cut-in maneuvers, this paper proposes a spatiotemporal predictive eco-cruising strategy (PECS) to address random cut-in maneuvers. The main contributions are summarized as follows: 1) A proactive eco-cruising control framework is developed for ECAVs under random cut-in maneuvers, which explicitly considers lateral stochastic disturbances caused by surrounding HDVs and enables ECAV presciently adjust driving speed. 2) A graph-based attention trajectory model (GATM) is

developed to predict the lane-change trajectories of HDVs. By modeling multi-vehicle interactions and incorporating a spatiotemporal attention mechanism, the proposed model effectively captures both spatial correlations and temporal dependencies, thereby improving the prediction accuracy of lane-change trajectory. 3) A trajectory-to-distance disturbance transformation mechanism is designed to convert predicted lane-change trajectories into future inter-vehicle distance disturbances, which are subsequently embedded into the MPC-based eco-cruising optimization to improve energy efficiency and travel efficiency. Furthermore, the effectiveness and robustness of the PECS are verified using real-world trajectory data.

The remainder of this paper is structured as follows: Section II introduces the traffic scenario investigated in this study, and establishes the vehicle energy consumption model. Section III presents the lane-change trajectory prediction model and performs vehicle ecological velocity optimization within an MPC framework. Section IV evaluates the proposed strategy through stochastic simulation and representative case analysis. Section V concludes the study and discusses future research.

II. PROBLEM STATEMENT AND MODELLING

In this section, the cut-in traffic scenarios and the corresponding eco-cruising OCP are first introduced, followed by the modeling of the vehicle energy consumption model.

A. Problem statement

In this study, ECAVs are assumed to acquire real-time information on surrounding vehicles and traffic conditions through onboard sensors, such as cameras, ultrasonic radar and millimeter-wave radar. The investigated scenario considers a three-lane straight road where HDVs may perform random lane-change maneuvers. Surrounding HDVs with potential lane-change intentions are referred to as the target vehicles. Note that all potential cut-in vehicles are treated as target vehicles for cut-in trajectory estimation. A representative cut-in scenario is illustrated in Fig. 2, where the ego vehicle is an ECAV surrounded by several other vehicles. The target vehicle, impeded by a slower-moving vehicle ahead, may develop an intention to change lanes to pursue higher travel efficiency. Obviously, the cut-in behavior of the target vehicle can cause a sudden reduction in the inter-vehicle distance of the ego vehicle, forcing sharp deceleration to ensure driving safety. A smaller post inter-vehicle distance requires more aggressive speed adjustments, resulting in pronounced velocity fluctuations that adversely affect

energy efficiency, ride comfort, and driving safety. The scope of this study is limited to longitudinal speed regulation of the ego vehicle and does not involve active lane-changing maneuvers.

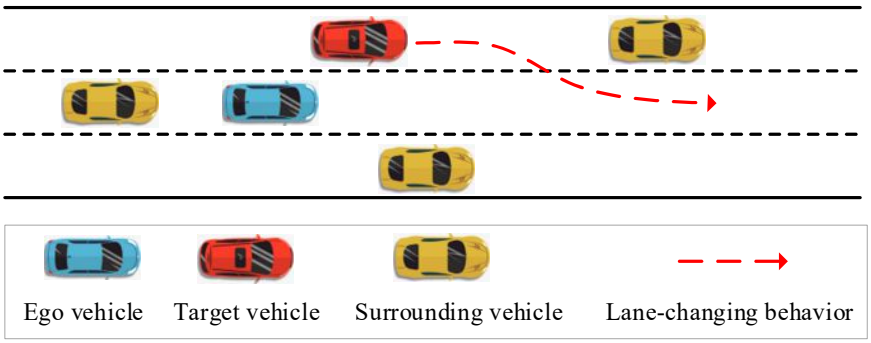


Fig. 2. The investigated scenario in this work.

The eco-cruising OCP in the cut-in scenarios aims to jointly optimize energy efficiency, travel efficiency and driving comfort under multiple constraints, including vehicle dynamics, speed limits, and safe inter-vehicle distance. Accordingly, the eco-cruising OCP in the cut-in scenario can be formulated, as:

$$\begin{aligned} &\min_{u} J(u,x) = w_1 J_{bat}(P_b) + w_2 J_{time}(v) + w_3 J_{comfort}(a) \\ &\text{s.t.} \quad a_{\min} \le a \le a_{\max} \\ &\qquad v_{\min} \le v \le v_{\max} \\ &\qquad d \ge d_s \end{aligned} \tag{1}$$

where J_{bat} is the energy consumption cost, which is calculated by integrating the battery power over the travel time, J_{time} represents the travel time cost, which is calculated by integrating the squared deviation between the ego vehicle speed and the average traffic flow speed over the travel time, $J_{comfort}$ is the cost functions for driving comfort, which is calculated by integrating the square of the jerk over the travel time, P_b denotes the battery power of the ego vehicle. The control and state variables are denoted by $u = a$ and $x = [v, d]$, respectively. The variable a denotes the vehicle acceleration, v is the vehicle speed, $a_{\min}$ and $a_{\max}$ are the minimum and maximum acceleration limits, $v_{\min}$ and $v_{\max}$ are the minimum and maximum speed limits, d is the inter-vehicle distance, d_s represents the desired inter-vehicle distance. The inter-vehicle distance and the desired inter-vehicle are formulated [36], as expressed:

$$d_s = H_s + T_s v \tag{2}$$

$$d(t) = s_p(t) - s(t) + \xi(t) \cdot \Delta d(t) \tag{3}$$

where H_s denotes the minimum inter-vehicle distance, T_s is the safe headway of the vehicle. s_p and s represent the position of the preceding vehicle and the ego vehicle, respectively. The indicator variable ξ equals 1 when a target vehicle executes a cut-in maneuver and 0 otherwise. Δd is the variation of inter-vehicle distance induced by the cut-in maneuver. It can be observed that a cut-in maneuver triggers an abrupt reduction in the inter-vehicle distance d, introducing a disturbance that causes a sudden change in the inter-vehicle distance constraint. The eco-cruising OCP must therefore be solved under these new constraints, which results remarkable variations in the optimal control decisions. Consequently, this ultimately degrades energy efficiency, driving comfort, and travel efficiency.

B. Vehicle model

To address the established eco-cruising OCP for ECAVs, the corresponding vehicle dynamics model and energy consumption model need to be constructed. Since the ego vehicle only performs longitudinal eco-cruising without active lane-changing maneuvers, a simplified longitudinal dynamics model is exploited to evaluate the proposed control framework, which is described as follows:

$$F_t = mgf\cos\theta + mg\sin\theta + \frac{1}{2}C_d A_v \rho v^2 + m\delta a \tag{4}$$

where F_t denotes the longitudinal force, m is the vehicle mass, g is the gravitational acceleration, f is the rolling resistance coefficient, the variable θ represents the road grade angle, C_d is the air resistance coefficient, A_v denotes the frontal area of the vehicle, ρ is the air density, and δ represents the vehicle rotational inertia coefficient. Given that the ECAV in this study adopts a centralized motor configuration, the output torque of the drive motor is given as follow:

$$T_m = \begin{cases} \dfrac{F_t r_w}{i_0 \eta_p} & F_t \geq 0 \\ \dfrac{F_t r_w}{i_0} \eta_p \xi & F_t \leq 0 \end{cases} \tag{5}$$

where T_m is the motor torque, r_w represents the wheel radius, the variable i_0 denotes the ratio of the final drive, η_b is the powertrain efficiency, and ξ indicates the torque distribution ratio for the regenerative braking motor, which is related to the regenerative braking strategy.

The motor power P_m is calculated based on the driving speed and motor torque. Due to the short duration in the cut-in processes, the effects of the battery SOC and internal resistance on energy consumption are neglected. Accordingly, the battery power P_b can be estimated by ignoring energy losses in wires, inverters, and converters. The battery power is calculated as follow:

$$N_m = \frac{60v}{2\pi r_w} \tag{6}$$

$$P_m = \frac{2\pi}{60} T_m N_m \tag{7}$$

$$P_b = P_m \eta_m^{-sign(T_m)}(N_m, T_m) \eta_b^{-sign(T_m)} \tag{8}$$

where N_m is the rotational speed of the motor, T_m is the motor torque, η_m indicates the motor efficiency, which is obtained from calibration experiments and determined by rotational speed and torque, and η_b denotes the battery efficiency, which is set as a constant.

III. ECO-CRUISING CONTROL STRATEGY CONSIDERING CUT-IN MANEUVERS

To mitigates the affection of random cut-in maneuvers, a spatiotemporal predictive eco-cruising control is developed to presciently estimate the variation in the inter-vehicle distance, thereby ensuring energy efficiency and comfort. This section details the prediction model combined with the proposed eco-cruising control strategy.

A. Control framework design

The unpredictable disturbances caused by HDVs in real-world driving environments poses significant challenges to accurately handling the variations in inter-vehicle distance, which is critical for solving the eco-cruising OCP. Moreover, driver styles and surrounding HDVs can significantly influence the lane-change trajectory, making it difficult to predict the cut-in trajectories. To address these issues, the spatiotemporal predictive eco-cruising control framework is developed that integrates lane-change trajectory prediction with eco-cruising control. As illustrated in Fig. 3, the proposed framework performs real-time velocity optimization using an MPC-based eco-cruising controller, which incorporates HDV lane-change trajectory predictions, the ego vehicle states and traffic information. The proposed framework operates within a hierarchical structure. At the high level, the GATM model combines a GCN to capture spatial interactions among HDVs with a transformer-based neural network to learn temporal dependencies from historical trajectory sequences. The pre-trained GATM model processes observations

over a given time window and predicts the target vehicle's lane-change trajectory over a specified prediction horizon. At the low level, the predicted trajectory is used to identify potential cut-in vehicles and estimate the variation in inter-vehicle distance over the prediction horizon. In this context, a multi-objective OCP is formulated to jointly optimize energy efficiency and travel efficiency while ensuring driving comfort. The eco-cruising OCP is further reformulated as a QP problem and efficiently solved within an MPC framework to enable real-time ecological velocity optimization. To explicitly account for high-risk cut-in scenarios in dense traffic, a safety-triggered switching mechanism is supplemented: when the cut-in position falls below a predefined threshold (e.g., 0.6 times the desired safe spacing) [37], the controller immediately overrides the nominal MPC-based eco-cruising mode and switches to an emergency braking mode to ensure collision avoidance.

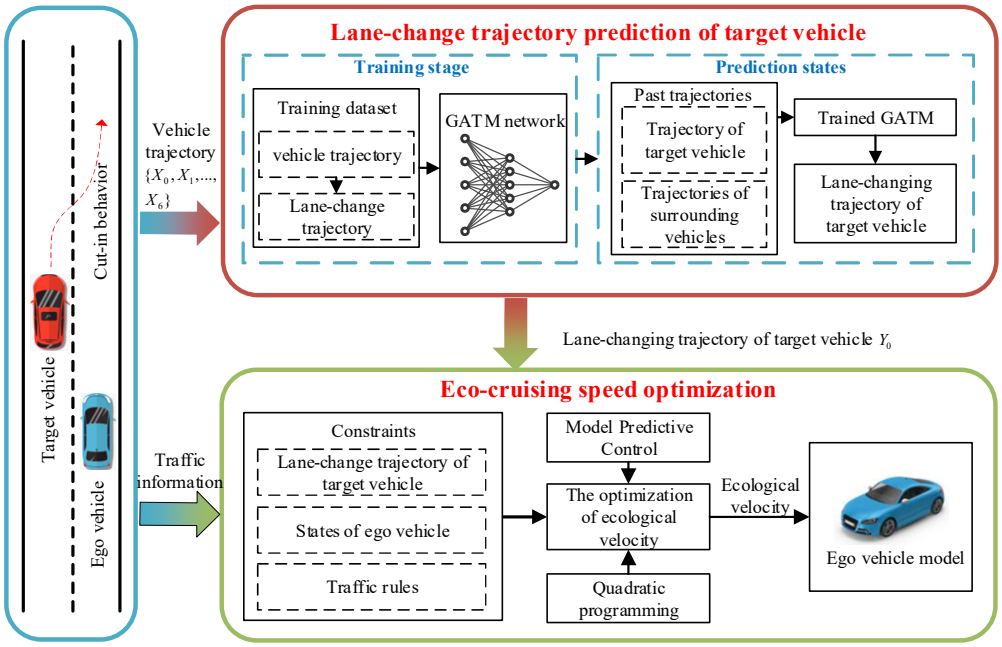


Fig. 3. The hierarchical control scheme of the PECS.

B. *Lane-change trajectory prediction model*

The motion trajectories of HDVs are mainly influenced by driving styles and interactions with surrounding vehicles, which can be represented through temporal and spatial features [29]. However, most existing studies typically utilize only one of these two types of features when predicting vehicle trajectories [38]. To jointly account for these two crucial factors, a trajectory prediction model is developed, as illustrated in Fig. 4. The model consists of dedicated spatial and temporal feature extraction layers designed to capture dynamic dependencies in both domains. In the spatial feature extraction layer, inter-vehicle interactions are modeled using GCNs, enabling the

extraction of topological relationships between the target vehicle and its surrounding vehicles. Furthermore, the multi-head attention mechanism is introduced to refine the spatial features by adaptively assigning different weights to surrounding vehicles according to their influence on the target vehicle. In the temporal feature extraction layer, a Transformer encoder is employed to capture long-range dependencies across consecutive time steps in the historical trajectories. Compared with recurrent structures, the attention-based temporal modeling mechanism can more effectively identify key historical moments that contribute to future lane-change motion. Therefore, a spatiotemporal attention mechanism is adopted to simultaneously capture the temporal dependencies embedded in the target vehicle's historical trajectory and the spatial dependencies arising from interactions with surrounding vehicles, thereby improving the prediction accuracy of lane-change trajectories.

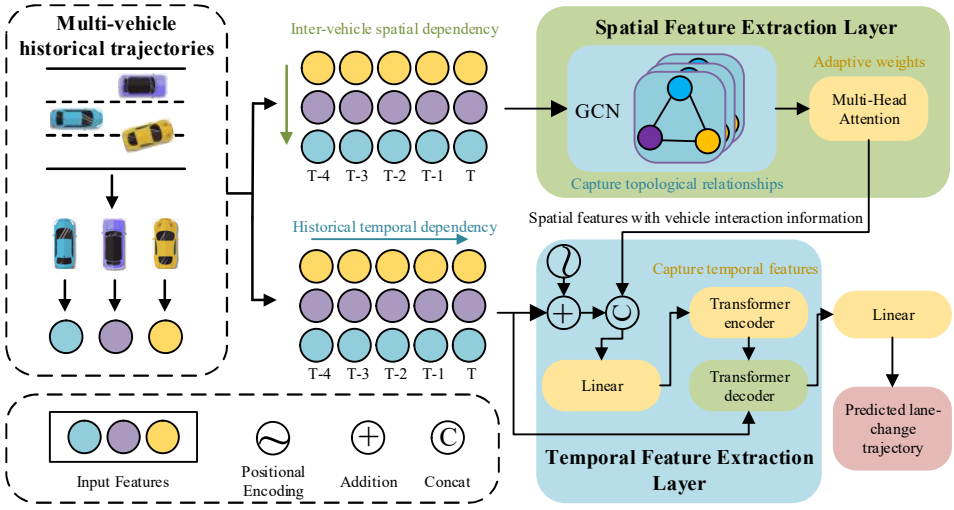


Fig. 4. Structure diagram of GATM vehicle trajectory prediction model.

Since any HDV surrounding the ego vehicle may potentially perform a lane-change maneuver, each surrounding HDV is treated as a candidate target vehicle. For each candidate, the historical trajectories of the target HDV and its neighboring vehicles are fed into the prediction model to forecast its future motion. Based on the predicted trajectories, potential cut-in vehicles are identified and their corresponding lane-change trajectories are generated. To accurately forecast the lane-change trajectories in complex environments, the driving states of seven vehicles, including the target vehicle and its surrounding vehicles, are extracted for the trajectory prediction. Specifically, these vehicles consist of the target vehicle, the two closest vehicles preceding and following it in the same lane, and the two nearest vehicles in the adjacent lanes. The spatial relationship of these seven vehicles is illustrated in Fig. 5.

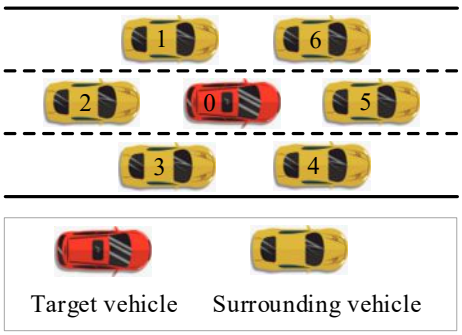


Fig. 5. Illustration of the target vehicle and its surrounding vehicle.

In this context, the historical motion trajectories of both the target vehicle and surrounding vehicles are used as the inputs to the prediction model, denoted as $X = \{X_0, X_1, ..., X_6\}$. The vehicle trajectory data in X contains the dynamic spatial interactions between any two vehicles during their travel. The historical trajectory of the vehicle i in X can be represented as:

$$X_i = \{X_i^{t_{obs}+1}, X_i^{t_{obs}+2}, ..., X_i^{t_{obs}+n}\} \tag{9}$$

where t_{obs} is the starting time index of the historical trajectory sequence. n represents the length of the observation window. At each time step *t*, the state of vehicle *i* is represented by $X_i^t = [x^t, y^t]$, which specifies the vehicle's centroid position in local coordinate frame, including the lateral position x^t and the longitudinal position y^t. Therefore, the sequence X_i represents the historical motion of vehicle *i* over a predefined observation window, explicitly encoding both the spatial positions and the temporal evolution of the vehicle trajectory, while inherently reflecting the vehicle's dynamic information, such as speed and acceleration. The model output corresponds to the prediction motion trajectory of target vehicle, expressed as:

$$\hat{Y} = \{\hat{Y}_0^1, \hat{Y}_0^2, ..., \hat{Y}_0^{t_{pred}}\} \tag{10}$$

where t_{pred} denotes the prediction horizon, and each frame $\hat{Y}_0^t = [\hat{x}_0^t, \hat{y}_0^t]$ represents to the predicted position of the target vehicle at time step *t*.

1) Spatial Feature Extraction Layer

The spatial feature extraction layer is designed to model spatial interactions among vehicles using GCN models. Specifically, based on the trajectory sequence X, the model derives the relative distances between the target vehicle and surrounding vehicles, as well as their temporal variations, to characterize inter-vehicle interactions. To

capture the spatial relationship among various vehicles, each vehicle is treated as a node, and the distance relationships among vehicles are defined as edges. As illustrated in Fig. 4, the spatial feature extraction layer is constructed by stacking several GCN layers followed by a multi-head attention layer.

The primary components of the graph include nodes and edges, through which interactions among vehicles are naturally represented. In the proposed framework, the GCN layers aggregate information from adjacent nodes based on trained weights and a predefined graph topology to generate node embeddings. Specially, a static graph $G=(V,E)$ is developed as the input data structure for the GCN layers, where V denotes the set of vertices corresponding to vehicles and $E=\left\{e_{i,j}^{t}\middle|i,j\in 0,1,...,6;t\in t_{obs},t_{obs}+1,...,t_{obs}+n\right\}$ represents the edges that encode the spatial relationships between vehicle i and vehicle j. When an interaction exists between vehicle *i* and *j* at time *t*, $e_{i,j}^{t}=1$; otherwise, $e_{i,j}^{t}=0$. Accordingly, the graph G is composed of a sequence of time-indexed graph state G_t, each characterizing vehicle interactions at time *t*. For each time step, the corresponding adjacency weights matrix $\mathbf{A_T}$ is defined as:

$$\mathbf{A_t}=\left\{a_{i,j}^{t}\middle|i,j=0,1,...,6;t=t_{obs},t_{obs}+1,...,t_{obs}+n\right\} \tag{11}$$

$$a_{i,j}^{t}=\tau_{j}^{t}-\tau_{i}^{t} \tag{12}$$

where $a_{i,j}^{t}$ represents the relative spatial displacement between vehicle i and vehicle j, τ_{j}^{t} denotes the two-dimensional coordinates of vehicle *j* at time step t. For the *l*-th layer, the standard graph convolution operation $\mathbf{H^{l+1}}$ is given by:

$$\overline{\mathbf{A}}_{\mathbf{t}}=\mathbf{D}_{\mathbf{t}}^{-\frac{1}{2}}(\mathbf{A}_{\mathbf{t}}+\mathbf{I})\mathbf{D}_{\mathbf{t}}^{-\frac{1}{2}} \tag{13}$$

$$\mathbf{H}^{\mathbf{l+1}}=\sum_{j=1}^{l}\mathbf{W}^{\mathbf{l}}\mathbf{H}^{\mathbf{j}}\overline{\mathbf{A}}_{\mathbf{t}} \tag{14}$$

where $\overline{\mathbf{A}}_{\mathbf{t}}$ is the normalized and weighted version of $\mathbf{A}_{\mathbf{t}}$, $\mathbf{D}_{\mathbf{t}}$ is the degree matrix, $\mathbf{I}$ denotes the identity matrix, $\mathbf{W^{l}}$ and $\mathbf{H^{j}}$ refer to the weight matrix and the output feature matrix at the layer l, respectively.

While GCNs are effective at capturing spatial features based on predefined graph structures, they are limited in explicitly modeling dynamic and adaptive spatial dependencies among vehicles at each time step. To address this

issue, a spatial transformation layer is developed to enhance representation of inter-vehicle interactions. Specifically, the input vector $\mathbf{E}^{'}$ is first projected into three latent subspaces through learnable linear transformations, yielding the query vector $\mathbf{q}_{\mathbf{i}}^{\mathbf{spa}}$, the key vector $\mathbf{k}_{\mathbf{i}}^{\mathbf{spa}}$, and the value vector $\mathbf{v}_{\mathbf{i}}^{\mathbf{spa}}$ matrices. These matrices are then processed using a multi-head attention mechanism to adaptively capture the pairwise spatial interactions among vehicles. Subsequently, the attention outputs are passed through a fully connected feed-forward network, followed by residual connections and layer normalization, resulting in the refined spatial interaction features. The overall spatial transformation process can be formulated as follows:

$$\mathbf{Z}^{'} = norm(\mathbf{H}_{\mathbf{i}}^{\mathbf{t}} + \mathbf{Z}) \tag{15}$$

$$\begin{cases} \mathbf{q}_{\mathbf{i}}^{\mathbf{spa}} = \mathbf{W}_{\mathbf{i}}^{\mathbf{q}} \cdot \mathbf{Z}^{'} \\ \mathbf{k}_{\mathbf{i}}^{\mathbf{spa}} = \mathbf{W}_{\mathbf{i}}^{\mathbf{k}} \cdot \mathbf{Z}^{'} \\ \mathbf{v}_{\mathbf{i}}^{\mathbf{spa}} = \mathbf{W}_{\mathbf{i}}^{\mathbf{v}} \cdot \mathbf{Z}^{'} \end{cases} \tag{16}$$

where $\mathbf{W}_{\mathbf{i}}^{\mathbf{q}}$, $\mathbf{W}_{\mathbf{i}}^{\mathbf{k}}$ and $\mathbf{W}_{\mathbf{i}}^{\mathbf{v}}$ are three learnable weight matrices in the spatial feature extraction layer, *norm* denotes normalization operation, and $\mathbf{Z}$ is the embedding of the observation sequence. Therefore, the output of the attention mechanism is given by:

$$Attention(\mathbf{q}_{\mathbf{i}}^{\mathbf{spa}}, \mathbf{k}_{\mathbf{i}}^{\mathbf{spa}}, \mathbf{v}_{\mathbf{i}}^{\mathbf{spa}}) = Soft\max\left(\frac{\mathbf{q}_{\mathbf{i}}^{\mathbf{spa}}(\mathbf{k}_{\mathbf{i}}^{\mathbf{spa}})^{\mathbf{T_a}}}{\sqrt{d_{ki}^{spa}}}\right)\mathbf{v}_{\mathbf{i}}^{\mathbf{spa}} \tag{17}$$

$$MultiHead(\mathbf{q}_{\mathbf{i}}^{\mathbf{spa}}, \mathbf{k}_{\mathbf{i}}^{\mathbf{spa}}, \mathbf{v}_{\mathbf{i}}^{\mathbf{spa}}) = Concat(Head_1^{spa}, ..., Head_i^{spa})\mathbf{W}_{\mathbf{spa}}^{\mathbf{0}} \tag{18}$$

$$Head_i^{spa} = Attention(\mathbf{q}_{\mathbf{i}}^{\mathbf{spa}}, \mathbf{k}_{\mathbf{i}}^{\mathbf{spa}}, \mathbf{v}_{\mathbf{i}}^{\mathbf{spa}}) \tag{19}$$

where $Head_i^{spa}$ denotes the *i*-th attention head in spatial feature extraction layer, d_{ki}^{spa} is the column dimension of matrix $\mathbf{q}_{\mathbf{i}}^{\mathbf{spa}}$, $\mathbf{W}_{\mathbf{spa}}^{\mathbf{0}}$ denotes the linear projection weight layer, operator "Concat" denotes the concatenation of the output matrices from all attention heads.

2) Temporal Feature Extraction Layer

The transformer encoder is employed to encode the vehicle trajectory sequence and extract temporal features. Subsequently, a fully connected layer is utilized to generate the predicted lane-changing trajectory of the target vehicle. As the core mechanism for capturing temporal features in the transformer, the self-attention mechanism

enables the model to capture dependencies between any two time steps in the sequence [39] and adaptively assign varying weights to each time step, thereby effectively characterizing the temporal evolution of vehicle lane-change trajectories.

The spatial interaction features extracted from the preceding layer are concatenated with the positionally encoded trajectory sequence to form the input vehicle vector $\mathbf{Z}_{cat}$. This vector is then processed through a multi-head attention mechanism to capture temporal dependencies, which is computed as:

$$\begin{cases} \mathbf{Q}_{\mathbf{i}}^{\mathbf{tem}} = \mathbf{W}_{\mathbf{i}}^{\mathbf{Q}} \cdot \mathbf{Z}_{cat} \\ \mathbf{K}_{\mathbf{i}}^{\mathbf{tem}} = \mathbf{W}_{\mathbf{i}}^{\mathbf{K}} \cdot \mathbf{Z}_{cat} \\ \mathbf{V}_{\mathbf{i}}^{\mathbf{tem}} = \mathbf{W}_{\mathbf{i}}^{\mathbf{V}} \cdot \mathbf{Z}_{cat} \end{cases} \tag{20}$$

where $\mathbf{W}_{\mathbf{i}}^{\mathbf{Q}}$, $\mathbf{W}_{\mathbf{i}}^{\mathbf{K}}$, and $\mathbf{W}_{\mathbf{i}}^{\mathbf{V}}$ represent three learnable weight matrices in the temporal feature extraction layer, $\mathbf{Q}_{\mathbf{i}}^{\mathbf{tem}}$, $\mathbf{K}_{\mathbf{i}}^{\mathbf{tem}}$ and $\mathbf{V}_{\mathbf{i}}^{\mathbf{tem}}$ indicate the query, key and value vector of the temporal feature extraction layer, respectively. The attention output is given by:

$$Attention(\mathbf{Q}_{\mathbf{i}}^{\mathbf{tem}}, \mathbf{K}_{\mathbf{i}}^{\mathbf{tem}}, \mathbf{V}_{\mathbf{i}}^{\mathbf{tem}}) = Soft\max\left(\frac{\mathbf{Q}_{\mathbf{i}}^{\mathbf{tem}} (\mathbf{K}_{\mathbf{i}}^{\mathbf{tem}})^{\mathbf{T_a}}}{\sqrt{d_{ki}^{tem}}}\right)\mathbf{V}_{\mathbf{i}}^{\mathbf{tem}} \tag{21}$$

$$MultiHead(\mathbf{Q}_{\mathbf{i}}^{\mathbf{tem}}, \mathbf{K}_{\mathbf{i}}^{\mathbf{tem}}, \mathbf{V}_{\mathbf{i}}^{\mathbf{tem}}) = Concat(Head_1^{tem}, ..., Head_i^{tem})\mathbf{W}_{\mathbf{tem}}^{\mathbf{0}} \tag{22}$$

$$Head_i^{tem} = Attention(\mathbf{Q}_{\mathbf{i}}^{\mathbf{tem}}, \mathbf{K}_{\mathbf{i}}^{\mathbf{tem}}, \mathbf{V}_{\mathbf{i}}^{\mathbf{tem}}) \tag{23}$$

where $Head_i^{tem}$ is the *i*-th attention head in temporal feature extraction layer, $i = 1, 2, ..., h$ denotes the number of attention heads, d_{ki}^{tem} represents the column dimension of matrix $\mathbf{Q}_{\mathbf{i}}^{\mathbf{tem}}$, and $\mathbf{W}_{\mathbf{tem}}^{\mathbf{0}}$ corresponds to the linear projection weight layer applied after concatenation.

C. Dataset and training

The Next Generation Simulation (NGSIM) dataset is utilized to develop the GATM model. Collected from two U.S. freeway segments and two arterial roadways, the NGSIM dataset constitutes a large-scale empirical microscopic traffic dataset that has been widely used by the research community [40]. In this study, data from the US Highway 101 section in Los Angeles, California is selected to construct the training data for developing prediction model.

To ensure adequate representation of different lane-change behaviors, a disproportionate stratified sampling

strategy is adopted to categorize dataset into three classes, including left lane-change, right lane-change, and straight-driving trajectories. Specially, each vehicle is treated as a target vehicle, and the dataset is first sorted by vehicle ID and timestamp. Lane-change events are identified by detecting changes in lane ID, and each event is labeled as either a left or right lane-change. For each identified lane-change event, the preceding and following vehicles are selected as surrounding vehicles based on whether they occupy the same or adjacent lanes and exhibit the minimum longitudinal distance to the target vehicle at the corresponding timestamp. A complete lane-change trajectory is then extracted, the complete maneuver trajectory is segmented into multiple samples using a six-second sliding temporal window. For each sample, the first two seconds of the trajectory are used as the observation sequence, while the subsequent four seconds are treated as the prediction horizon. The 2 s observation window captures recent motion information while avoiding irrelevant long-term history. The 4 s prediction horizon covers the main evolution of lane-change maneuvers and provides sufficient look-ahead information for subsequent eco-speed optimization. In contrast, an excessively long prediction horizon may increase prediction uncertainty and computational burden [41]. For straight-driving trajectories, multiple six-second trajectory samples are similarly extracted from longer continuous driving sequences without any lane-change behavior. The surrounding vehicles are determined using the same selection criteria as those applied in the lane-change scenarios.

A fixed number of samples are systematically selected from each class to construct a balanced dataset. A total of 400 trajectories and their surrounding data are collected, including 133 left lane-changing trajectories, 133 right lane-changing trajectories, and 134 straight-driving trajectories. From these three categories, 80% of the samples are randomly assigned to the training set, while the remaining 20% are used for testing. Each target vehicle's trajectory and its surrounding vehicles' trajectories are processed into numerous data sequences of six seconds, in which the first two seconds are set as the inputs and the subsequent four seconds are defined as the outputs [42]. Fig. 6 illustrates the average speed distribution of 400 trajectories in the dataset. The distribution peaks at around 24 km/h and spans a range from 3 km/h to 60 km/h. This range encompasses trajectory data from various traffic states, from congested to free flow conditions, which enables the lane-change prediction model to learn more comprehensive behavioral features associated with speed and enhances its generalizability across diverse traffic scenarios.

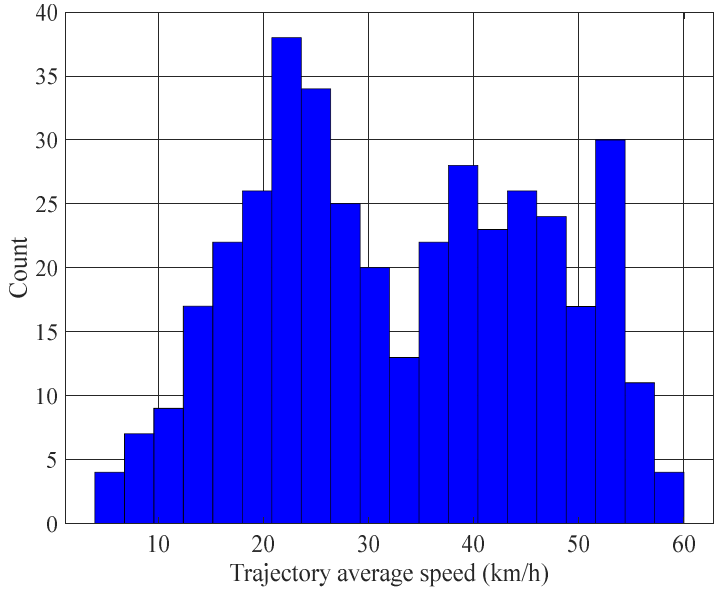


Fig. 6. Speed distribution of the trajectories.

D. The optimization of ecological velocity

To integrate the lane-change trajectory prediction into the eco-cruising control strategy, an MPC framework is utilized with discretized vehicle states. Assuming that the vehicle state remains constant during each sampling period Δt, the discrete state-space equation with disturbance terms is formulated as:

$$\mathbf{x}(k+1) = \mathbf{A}\mathbf{x}(k) + \mathbf{B}u(k) + \mathbf{M}z(k) \tag{24}$$

$$\mathbf{x}(k) = \begin{bmatrix} d(k) \\ v(k) \end{bmatrix}, u(k) = a(k), \mathbf{z}(k) = \begin{bmatrix} \Delta d(k) \\ v_p(k) \end{bmatrix} \tag{25}$$

and the system matrices are given by:

$$\mathbf{A} = \begin{bmatrix} 1 & -\Delta t \\ 0 & 1 \end{bmatrix}, \mathbf{B} = \begin{bmatrix} -\frac{1}{2}\Delta t^2 \\ \Delta t \end{bmatrix}, \mathbf{M} = \begin{bmatrix} 1 & \Delta t \\ 0 & 0 \end{bmatrix} \tag{26}$$

where $v_p(k)$ denotes the velocity of the preceding vehicle. Since the optimization is performed in a rolling-horizon manner with a short sampling interval, the speed variation of preceding vehicle within each time step is relatively small. Therefore, the acceleration of the preceding vehicle is neglected to simplify the calculation of the inter-vehicle distance $d(k)$, and the inter-vehicle distance is approximated:

$$d(k+1) = d(k) + v_p(k)\Delta t - (v(k)\Delta t + \frac{1}{2}a(k)\Delta t^2) + \Delta d(k) \tag{27}$$

where $\Delta d(k) = 0$ applies in the absence of a target vehicle cut-in. When a target vehicle cuts into the ego lane (i.e., crosses the lane marking) and a rolling optimization is performed, the variation in inter-vehicle distance is updated according to:

$$\Delta d(k) = -\left[s_p(k+\mu|k) - s_{cv}(k+\mu|\mathrm{k}) \right] \tag{28}$$

where μ denotes the time step at which the cut-in vehicle crosses the lane marker. s_p and s_{cv} represent the positions of the preceding vehicle and the cut-in vehicle, respectively, which are obtained from the lane-change trajectories predicted by GATM. The objective function for velocity optimization is designed to simultaneously optimize energy efficiency, travel efficiency and safety. In addition, smoother driving behavior is indirectly encouraged during the energy-efficient velocity optimization process, which helps reduce acceleration fluctuations and acceleration peak. The objective function is expressed as follows:

$$\min_{a_{k|k},\ldots,a_{k+N-1|k}} \sum_{j=0}^{N-1} \left\{ q_1 P_b(k+j|k)\Delta t + q_2[v(k+j|k) - V^*]^2 + q_3 \varepsilon(k+j|k) \right\} \tag{29}$$

where N denotes the prediction horizon of the MPC, V^* is the average traffic flow velocity, and ε is the slack variable. The parameters q_1, q_2, and q_3 are positive weighting factors associated with energy consumption, velocity deviation, and inter-vehicle distance, respectively. The first term minimizes the battery energy consumption, the second term encourages the optimized vehicle velocity to track the average traffic flow velocity, and the third term enforces safety by penalizing violations of the minimum inter-vehicle distance during cut-in scenarios.

QP algorithm is leveraged to solve the ecological velocity OCP while maintaining computational efficiency. As the battery power P_b in Equation (8) incorporates a nonlinear motor efficiency map, resulting in a high-dimensional nonlinear function. In this context, the expression for battery power can be approximated as a polynomial [43]. The resulting fitted polynomial is given by:

$$P_b(v(k), a(k)) = \sum_{i=0}^{3} \sum_{j=0}^{2} \omega_{ij} v^i(k) a^j(k) \tag{30}$$

where the parameters ω_{ij} are the polynomial fitting coefficients, which can be acquired offline via a linear least squares polynomial fitter. The fitting results and the fitting error are presented in Fig. 7 and Fig. 8, respectively. The polynomial approximation achieves a high goodness-of-fit, with an R^2 value of 0.994, which is close to unity over

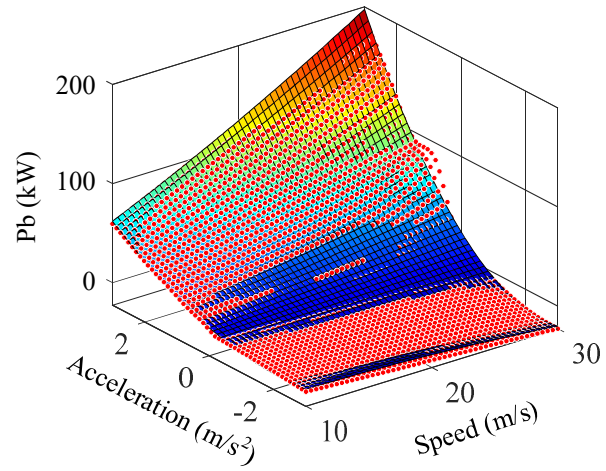


Fig. 7. The fitting result of battery power.

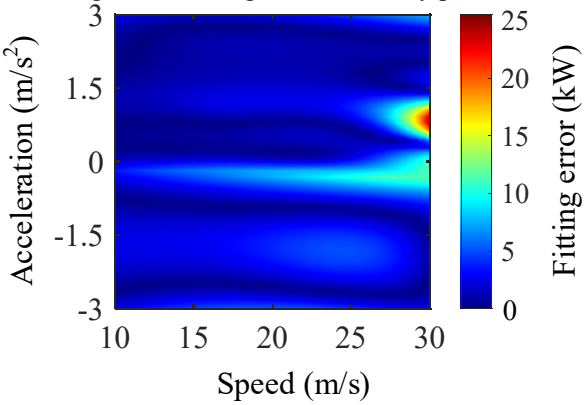


Fig. 8. The fitting error of battery power.

the considered operating region. The median fitting error is 1.73 kW, indicating that the model maintains good accuracy across most of the operating envelope. Despite the localized fitting deviation, its impact on the optimal control solution is limited, as the MPC-based optimization is primarily influenced by relative cost variations rather than absolute power values. Therefore, the proposed polynomial approximation achieves sufficient accuracy for eco-cruising optimization purposes [44]. To further reduce computational burden and express vehicle energy consumption in a form suitable for QP, Equation (30) is simplified by incorporating the velocity from the previous time step into the higher-order terms. As a result, the energy consumption is approximated by the following quadratic polynomial:

$$\begin{aligned} P_b(v(k),a(k)) = {} & \omega_{30}\overline{v}v^2(k) + \omega_{21}\overline{v}v(k)a(k) + \omega_{12}\overline{v}a^2(k) + \omega_{20}v^2(k) \\ & + \omega_{11}v(k)a(k) + \omega_{02}a^2(k) + \omega_{10}v(k) + \omega_{01}a(k) + \omega_{00} \end{aligned} \tag{31}$$

where the specific values of polynomial fitting coefficients are provided in Table 1.

To ensure driving safety, the inter-vehicle distance is constrained to above a prescribed safe threshold. Accordingly, the following constraint is imposed in the optimization problem:

$$d_s(k+j\,|\,k)-\varepsilon(k+j\,|\,k)\le d(k+j\,|\,k) \tag{32}$$

where $d_s(k+j\,|\,k)$ is the safe inter-vehicle distance calculated by Equation (2), and $d(k+j\,|\,k)$ is the actual inter-vehicle distance derived from Equation (27). The vehicle speed must be non-negative and must not exceed the road speed limit $v_{\max}$. In addition, to ensure driving comfort, the acceleration magnitude is also constrained as follow:

$$0\le v(k+j\,|\,k)\le v_{\max} \tag{33}$$

$$a_{\min}\le a(k+j\,|\,k)\le a_{\max} \tag{34}$$

Table 1 Parameters of fitted battery power function.

Parameter	Value	Parameter	Value
ω_{32}	0	ω_{11}	683.2
ω_{31}	0	ω_{10}	459.8
ω_{30}	0.03184	ω_{02}	206.1
ω_{21}	14.17	ω_{01}	3001
ω_{20}	10.48	ω_{00}	-61.46
ω_{12}	232.3		

IV. VALIDATION

To validate the performance of the proposed method, both the prediction model and the eco-cruising strategy are systematically tested and analyzed. The proposed GATM model is implemented and evaluated using the deep learning framework Pytorch 2.5.1 with CUDA 11.8. Meanwhile, stochastic simulations and typical case studies for the proposed PECS are carried out on the MATLAB platform (version 24.1, R2024a). All validations are performed on a computer equipped with an Intel(R) Core(TM) i5-14600KF processor, an NVIDIA GeForce RTX 4060 GPU, and 32 GB of RAM.

A. Simulation setup

To analyze and evaluate the performance of the proposed PECS, comparative analyses are conducted against three benchmark strategies, with their core parameters kept consistent to ensure a fair comparison. The basic vehicle parameters used for validation are derived from CarSim (version 2020.0), and the corresponding parameters are listed in Table 2. The regenerative braking motor torque distribution ratio is set to 0.3. The initial SOC is set to 0.6, and SOC variation is neglected due to the short duration of cut-in events.

Table 2 Basic parameters of the vehicle.

Parameter	Value	Parameter	Value
Vehicle mass m	1235.9 kg	Final drive ratio i_0	7.94
Gravitational acceleration g	9.8 m/s^2	Powertrain efficiency η_p	0.9
Rolling resistance coefficient f	0.015	Maximum acceleration $a_{\max}$	2 m/s^2
Air drag coefficient C_d	0.3	Maximum deceleration $a_{\min}$	-5 m/s^2
Front area A_v	1.6 m^2	Maximum motor power	165 kW
Air density ρ	1.206 kg/m^3	Maximum motor torque	305 N□m
Rotational inertia coefficient δ	1.022	Perception range of onboard sensors	200 m
Tire radius r_w	0.298 m	Battery efficiency η_b	0.9

The first benchmark is a baseline strategy based on the Intelligent Driver Model (IDM), which is employed to emulate human driving behavior. The IDM is configured with a minimum following distance of 50 m, a desired time headway of 1.5 s, a maximum comfortable deceleration of –2 m/s², and a maximum deceleration of –5 m/s² [45]. The second benchmark strategy is a conventional eco-cruising strategy (denoted as QECS), which is developed based on MPC and QP without incorporating lane-change prediction. In QECS, velocity optimization is only triggered after the cut-in vehicle has completed the lane-change maneuver and becomes the immediate preceding vehicle of the ego vehicle. In contrast, the proposed PECS explicitly predicts the cut-in behavior in advance and performs proactive ecological speed optimization during the lane-change process. To isolate the contribution of lane-change prediction, QECS shares the same controller structure and parameter settings as the proposed PECS. The third benchmark is a machine learning-based eco-cruising strategy (simplified as LECS), which predicts lane-change behaviors via a BiLSTM-based model and integrates the prediction results into the eco-cruising control framework. The BiLSTM model is formulated as:

$$\hat{Y}_{tar} = f_{BiLSTM}(X_{tar}) \tag{35}$$

where f_{BiLSTM} represents the lane-change trajectory prediction model based on BiLSTM, $X_{tar} = \{X_{tar}^{t_{obs}+1}, X_{tar}^{t_{obs}+2}, ..., X_{tar}^{t_{obs}+n_{obs}}\}$ denote the historical trajectory of the target vehicle within a predefined observation window n_{obs} of 40 time steps. Each frame $X_{tar}^{t} = [x^t, y^t]$ represents to the historical position of the target vehicle at time step *t*. $\hat{Y}_{tar} = \{\hat{Y}_{tar}^{1}, \hat{Y}_{tar}^{2}, ..., \hat{Y}_{tar}^{t_{pred}}\}$ is the predicted motion trajectory of the target vehicle from

the BiLSTM model with a prediction horizon t_{pred} of 40 time steps, and each frame $\hat{Y}_{tar}^{t} = [\hat{x}^{t}, \hat{y}^{t}]$ is the predicted position of the target vehicle at time step *t*. The BiLSTM model processes sequential data by combining both forward and backward LSTM networks, enabling it to capture temporal features from historical trajectories [46].

To evaluate the sensitivity of prediction horizon, the proposed PECS is compared with the baseline strategy under 40 real world cut-in scenarios. The results under different prediction horizons are presented in Fig. 9. As the prediction horizon increases from 1 s to 4 s, the energy efficiency improvement rises significantly from 8.21% to 17.04%. However, further extending the horizon to 5 s yields only slight additional improvement while increasing trajectory prediction errors and computational burden. Therefore, the prediction horizon is selected to 4 s balance energy efficiency, prediction accuracy, and computational efficiency.

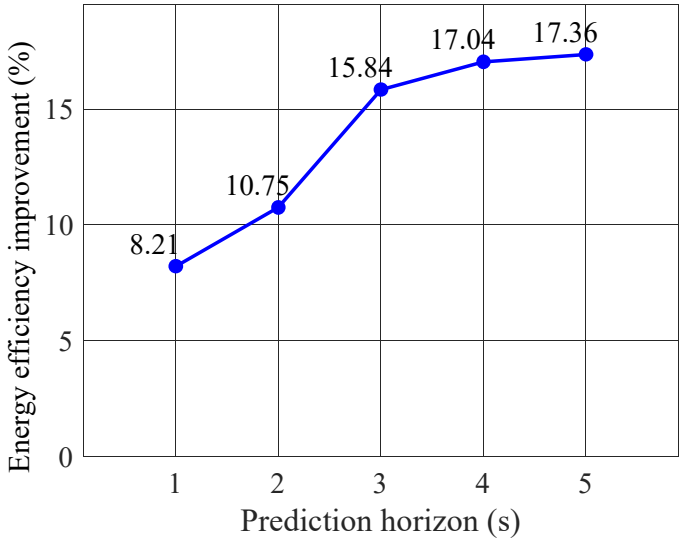


Fig. 9. Average performance analysis of the PECS under different prediction horizons.

The parameters used for training the GATM and implementing the MPC are summarized in Table 3. These parameters are determined through iterative tuning to balance prediction accuracy, control performance, and computational efficiency. In particular, the learning rate affects the convergence stability of GATM training, while the number of attention heads influences the capability of capturing spatial interaction features. Increasing the number of attention heads can enhance interaction modeling but also increases computational complexity and the risk of overfitting. Therefore, the final parameter settings are selected by jointly considering model accuracy and inference efficiency.

Table 3 The parameters of the GATM and MPC.

Parameter	Value	Parameter	Value
Hidden layer size	128	Energy consumption weight q_1	0.05
Batch size	64	Travel efficiency weight q_2	1.4
Initial learning rate	0.001	Driving safety weight q_3	12
Weight decay	10^{-4}	The prediction horizon N_{MPC} of MPC	20 s
Dropout rate	0.1	Sampling time	0.1 s
The number of heads for multi-head attention	8	Time headway	1.5 s
The epochs of training	200	The minimum and maximum speed limits	15 km/h / 100 km/h
The number of decoder and encoder layer	12	The length of observation window n	20
The prediction horizon of GATM t_{pred}	40		

B. Lane-change trajectory prediction analysis

To validate the prediction performance of the proposed GATM model, comparisons with BiLSTM and Transformer models are conducted through the real-world data from the NGSIM dataset. Three indexes are used to evaluate the performance of trajectory prediction models including, the average displacement error (ADE), final displacement error (FDE), and miss rate (MR). Among these indexes, the ADE measures the overall accuracy of over the entire predicted trajectory and is defined as:

$$ADE = \frac{1}{N_{tra}} \frac{1}{t_{pred}} \sum_{i=1}^{N_{tra}} \sum_{t=1}^{t_{pred}} \left\| \hat{Y}_i^t - Y_i^t \right\|_2 \tag{36}$$

where N_{tra} denotes the number of the lane-change trajectories, Y_i^t is the real future trajectory of the *i*-th sample, $\hat{Y}_i^t$ indicates corresponding predicted trajectory. The FDE is defined as the error between the predicted and the actual final positions of the lane-change. It is designed to evaluate the accuracy of endpoint position prediction which is calculated as follows:

$$FDE = \frac{1}{N_{tra}} \sum_{i=1}^{N_{tra}} \left\| \hat{Y}_i^{t_{pred}} - Y_i^{t_{pred}} \right\|_2 \tag{37}$$

where $Y_i^{t_{pred}}$ and $\hat{Y}_i^{t_{pred}}$ denote the real and predicted endpoint position of the *i*-th trajectory. The MR is defined

as the proportion of predicted trajectories whose final positions error exceeds 2 meters, reflecting the validity and reliability of the predicted trajectories.

To validate the prediction performance using real-world trajectory data, 80 lane-change cases from the NGSIM dataset are used to evaluate the proposed GATM model. The average prediction performance of the three prediction models is presented in Fig. 10. It can be found that the proposed GATM model remarkably outperforms the BiLSTM model across all three metrics, achieving improvements of 67.9%, 71.0%, and 73.6% in ADE, FDE, MR, respectively. Compared with the Transformer model, the proposed GATM model also achieves improvements of 24.74%, 17.91%, and 28.63% in ADE, FDE, and MR, respectively. These results demonstrate that, by effectively capturing spatiotemporal features, the GATM model yields more accurate predictions of future lane-change trajectories and final positions. Moreover, GATM achieves a low MR of only 0.172, indicating more stable predictions with fewer invalid outcomes.

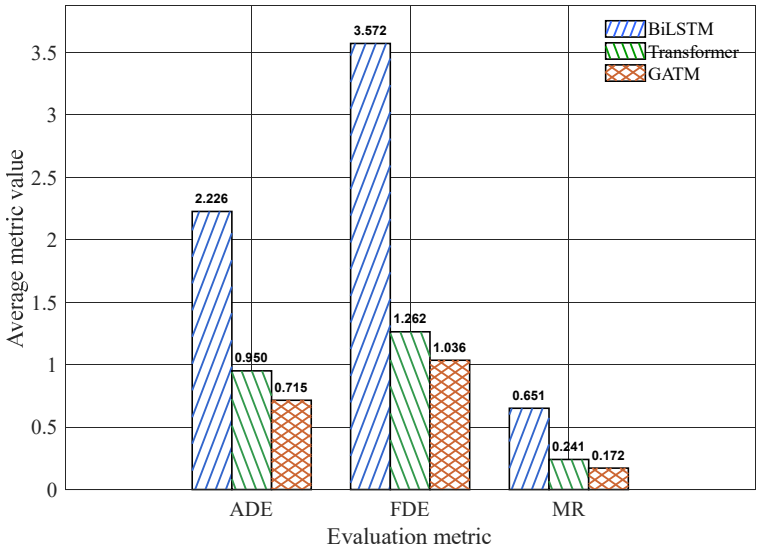
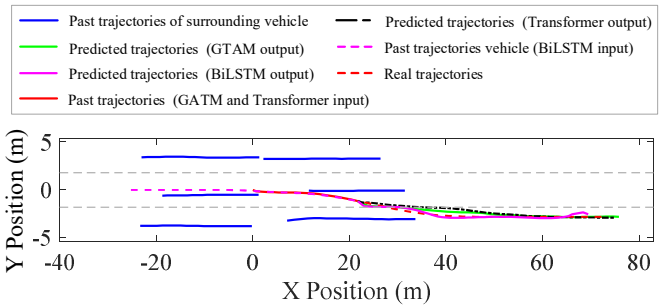


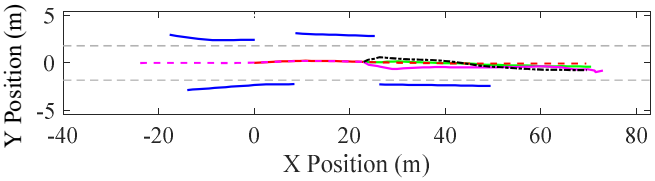
Fig. 10. Comparative experiments on the test set.

Specifically, Fig. 11 presents the prediction results of the GATM and BiLSTM models under three scenarios: straight-driving, left lane-change, and right lane-change. The GATM model demonstrates superior performance across all three scenarios. The predicted trajectories exhibit high consistency with the real motion trajectory and exhibit smooth, natural curvature. In contrast, the BiLSTM model generates trajectories with noticeable initial deviations, along with excessive local oscillations. Although the trajectory predicted by the Transformer model is also relatively smooth, the trajectory generated by the GATM model aligns more closely with the real motion trajectory. Additionally, the GATM model accurately predicts the final cut-in positions in all three scenarios, with a

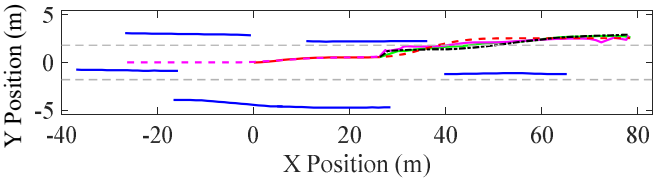
maximum error of 2 m, which improves inter-vehicle distance estimation and supports more effective eco-cruising control. By comparison, the BiLSTM model exhibits significantly larger endpoint errors, reaching up to 5 m in the longitudinal direction during right lane-change prediction, as illustrated in Fig. 11(a). The average inference times are 1 ms, 3.29 ms, and 4.84 ms for the BiLSTM, Transformer, and GATM models, respectively. Although GATM incurs a slightly more time due to its more complex architecture, it delivers notably improved trajectory prediction accuracy. Importantly, the inference time remains within the millisecond scale, indicating that the proposed model is computationally efficient and suitable for real-time applications. In summary, by leveraging spatiotemporal features, the proposed GATM model achieves high-accuracy lane-change trajectory prediction in both trajectory consistency and endpoint precision while maintaining preferable computational efficiency.



(a) Right lane-change scenario



(b) Straight-line driving scenario



(c) Left lane-change scenario

Fig. 11. Lane-changing trajectory schematic.

To analyze the contributions of the spatial feature extraction layer and the temporal feature extraction layer in GATM, ablation experiments are conducted under different prediction horizons. Table 4 presents the RMSEs of the ablation experiments across different prediction horizons ranging from 1 s to 5 s. To eliminate the influence of irrelevant variables, the removed spatial or temporal feature extraction layer is replaced with fully connected layers of the same size. As shown in Table 4, the complete GATM achieves the lowest RMSE across all prediction horizons,

indicating that both the spatial and temporal feature extraction layers contribute positively to vehicle trajectory prediction performance. When the spatial feature extraction layer is removed, the RMSE increases across all prediction horizons. In particular, at the 4 s prediction horizons, the RMSE remarkably increases by 17.74% compared with the complete GATM model. This result indicates that spatial interaction information plays an important role in accurate motion prediction. When the temporal feature extraction layer is removed, the prediction accuracy degradation becomes more pronounced, especially for longer prediction horizons. This indicates that the temporal feature extraction layer is critical for capturing long-term dependencies and improving the stability and accuracy of long-horizon trajectory prediction.

Table 4 The results of RMSE for ablation experiments under different prediction horizons.

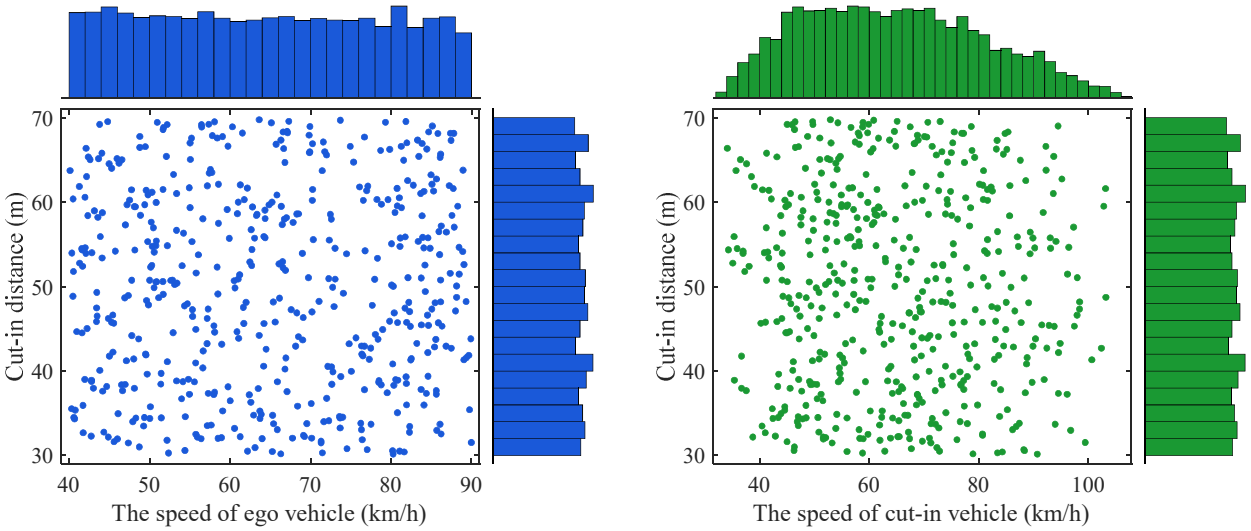
Prediction Horizon (s)	1	2	3	4	5
GATM	0.365	0.538	0.637	0.834	1.241
GATM without spatial feature extraction layer	0.379	0.581	0.721	0.982	1.394
GATM without temporal feature extraction layer	0.383	0.597	0.845	1.170	1.586

C. Stochastic simulation analysis

To evaluate the robustness and generalizability of the proposed eco-cruising strategy, extensive stochastic simulations are conducted over 5000 randomly generated cut-in scenarios. Each cut-in scenario is constructed based on three randomized parameters that characterize the interaction intensity between the ego vehicle and the cut-in vehicle. Specifically, the initial speed of the ego vehicle is sampled from 40–90 km/h, the speed of the cut-in vehicle is set to 0.8–1.2 times that of the ego vehicle, and the cut-in position is randomly assigned within 30–70 m ahead of the ego vehicle. By varying these parameters, the generated scenarios can effectively represent cut-in maneuvers with different disturbance levels and risk intensities under diverse traffic conditions. The specific distributions of the three random parameters used to construct the cut-in scenarios are shown in Fig. 12.

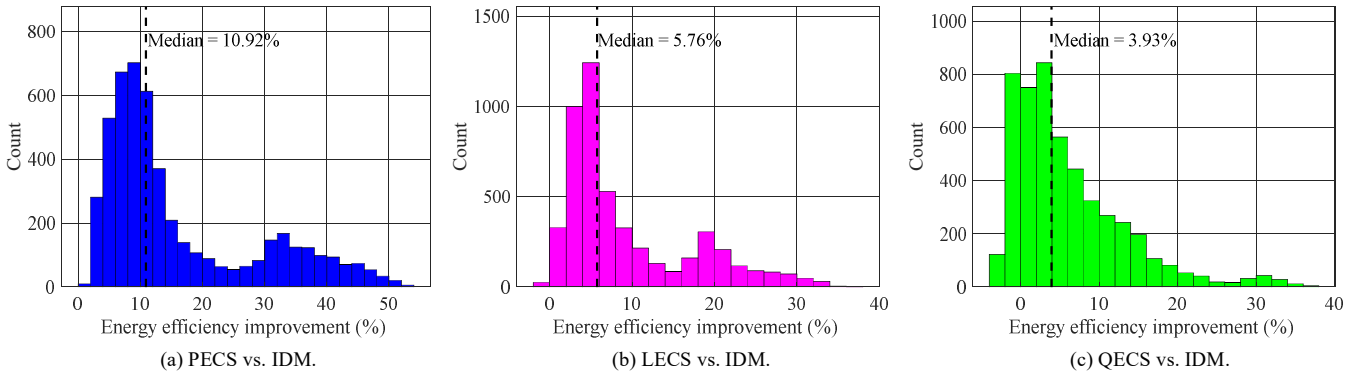
Fig. 13 illustrates the average energy efficiency improvement of each strategy compared with the baseline benchmark. The energy consumption is defined as the sum of the battery energy consumption and the equivalent electrical energy consumption associated with the kinetic energy difference between the initial and finial states. The energy efficiency improvement achieved by PECS is most frequently concentrated around the median value of 10.92%, whereas the corresponding improvements for LECS and QECS are 5.76% and 3.93%, respectively. Furthermore, the maximum energy efficiency improvement achieved by the PECS reaches 55%, significantly

exceeding the 35% upper bound observed for both the LECS and QECS methods. These findings demonstrate that the superior energy efficiency of the proposed PECS under stochastic cut-in conditions.



(a) The ego vehicle speed and cut-in distance distribution (b) The cut-in vehicle speed and cut-in distance distribution

Fig. 12. Parameter distribution of random cut-in scenarios.



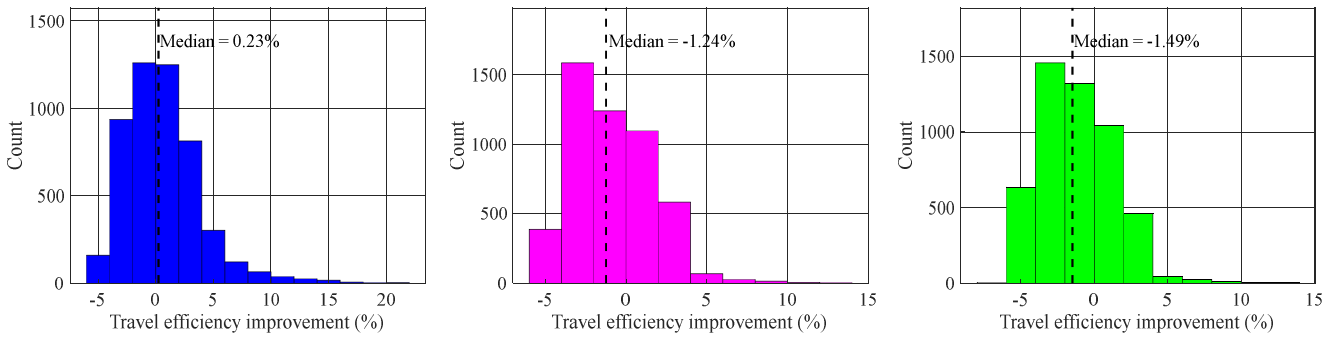
(a) PECS vs. IDM. (b) LECS vs. IDM. (c) QECS vs. IDM.

Fig. 13. Energy efficiency improvement of different strategies during 5,000 stochastic simulations.

Travel efficiency is evaluated using the average speed of the ego vehicle. As shown in Fig. 14, the travel-efficiency improvement of PECS is mainly distributed around the median value of 0.23%, whereas both the LECS and QECS exhibit negative median value of travel efficiency enhancement. This indicates that the PECS effectively reduces energy consumption without sacrificing travel efficiency, while both the LECS and QECS incur a certain degree of travel efficiency degradation.

To investigate the influence of cut-in position on the eco-cruising performance, the energy efficiency improvements of the three eco-cruising strategies are analyzed, as shown in Fig. 15. Across all cut-in distances, the proposed PECS achieves the highest energy efficiency improvement. Moreover, the energy efficiency improvement

of the PECS increases as the cut-in distance decreases, indicating stronger benefits in short-distance cut-in scenarios. As the cut-in distance increases, the influence of the cut-in maneuver weakens, resulting in increasingly similar performance across the three strategies. Due to the lower lane-change prediction accuracy, the energy efficiency improvement of the LECS shows slight correlation with changes in cut-in distance.



(a) PECS vs. IDM. (b) LECS vs. IDM. (c) QECS vs. IDM.

Fig. 14. Travel efficiency improvement of different strategies during 5,000 stochastic simulations.

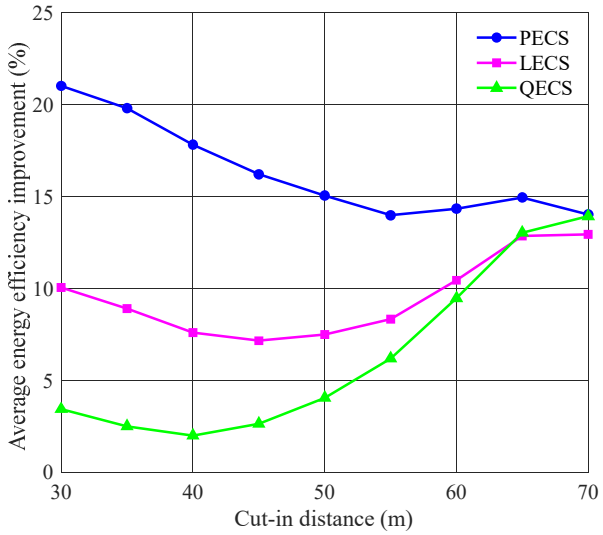


Fig. 15. Distribution of energy efficiency improvement dependence on cut-in distance.

The average energy efficiency improvement and average travel efficiency improvement for each strategy across the 5000 stochastic simulations are summarized in Table 5. Compared with the IDM method, the proposed PECS achieved the highest average energy efficiency improvements of 16.23%, significantly outperforming the other benchmark methods. In addition, the average travel efficiency improvement of the PECS is 0.60%, indicating no noticeable deterioration in travel efficiency under random cut-in maneuvers. Moreover, the PECS achieves a mean maximum jerk of 1.74 m/s^3, reflecting a significant improvement in driving comfort. In terms of computational efficiency, the IDM has the lowest computation time of 2.00 ms due to its rule-based structure. The

QECS and LECS require 8.73 ms and 9.05 ms, respectively, while PECS requires 12.95 ms because of the additional lane-change prediction module. Although PECS exhibits slightly higher computational cost, it remains within the millisecond level. This indicates that the proposed method maintains real-time capability without significant computational burden. Overall, PECS achieves a favorable balance between energy efficiency, driving comfort, and computational efficiency.

Table 5 Results of stochastic simulation.

Strategy	Average energy efficiency improvement (%)	Average travel efficiency improvement (%)	Average of max jerk (m/s³)
IDM	-	-	14.23
QECS	6.04	-1.17	6.69
LECS	9.27	-0.88	5.12
PECS	16.23	0.60	1.74

D. Representative case analysis

To systematically evaluate the performance of the proposed strategy under different cut-in scenarios, four real cut-in cases are selected from the NGSIM dataset for analysis. To reproduce real cut-in scenarios, the ego vehicle's initial speed, the initial cut-in position, and the target vehicle's lane-change trajectory are extracted from real-world data. As summarized in Table 6, four cases are defined, labeled Case 1 to Case 4. Case 1 and Case 2 exhibit relatively short cut-in distances, whereas the distances in Case 3 and Case 4 increase progressively. Although Case 2 and Case 3 differ in cut-in position, their cut-in speeds are comparable, enabling a clearer assessment of the influence of distance under similar speed conditions. Overall, both the initial cut-in position and cut-in speed are varied to comprehensively evaluate the proposed method in different cut-in scenarios.

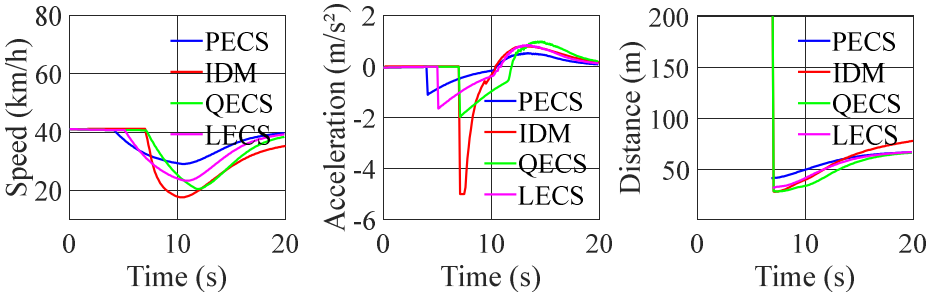
Table 6 Parameters of representative cases.

Parameters	**Case 1**	**Case 2**	**Case 3**	**Case 4**
Initial speed of ego vehicle	41.1 km/h	60.2 km/h	58.9 km/h	49.2 km/h
Initial cut-in position	31.4 m	32.5 m	44.1 m	52.5 m
Initial cut-in speed	39.6 km/h	51.7 km/h	52.9 km/h	49.5 km/h

The velocity profiles of Case 1, which evaluates the performance under a small cut-in distance, are illustrated in Fig. 16(a). All four strategies decelerate in response to the cut-in maneuver occurring with a limited initial inter-vehicle distance. Among them, the PECS and the LECS leverage lane-change trajectory predictions to anticipate the cut-in maneuver in advance, enabling earlier speed adjustments compared with the other two strategies. Benefiting from higher prediction accuracy, the PECS initiates deceleration earlier and more smoothly than LECS, resulting in reduced speed fluctuations. This smoother velocity evolution contributes to improved energy efficiency and driving comfort. Fig. 16 (b) presents the acceleration profiles of the four strategies in Case 1. The PECS exhibits

the smallest peak deceleration of only –1.11 m/s², compared with the other three strategies. These results further demonstrate its superiority in driving comfort. Additionally, Fig. 16(c) verifies that all strategies successfully maintain a safe inter-vehicle distance throughout the cut-in scenario, thereby avoiding any potential risk of a rear-end collision.

To evaluate robustness under realistic perception imperfections, missed detections are simulated by randomly removing 10%, 20%, and 30% of historical trajectory data, with the gaps filled via linear interpolation. As shown in Table 7, the energy-saving improvement decreases moderately from 23.72% to 20.87% as the data loss increases to 30%, while the PECS still maintains clear advantages over the IDM. To further simulate sensor measurement errors, zero-mean Gaussian disturbances are added to the vehicle historical position trajectories [47]. Two noise scenarios with different variances of 0.001 and 0.005 are selected. Under high-level Gaussian noise, the proposed PECS still achieves a 21.31% improvement in energy efficiency. Meanwhile, no noticeable deterioration in inter-vehicle distance is observed. These results indicate that the proposed strategy exhibits good robustness in both energy efficiency and safety under imperfect sensing conditions.



(a) Vehicle speed. (b) Vehicle Acceleration. (c) Intervehicle distance.

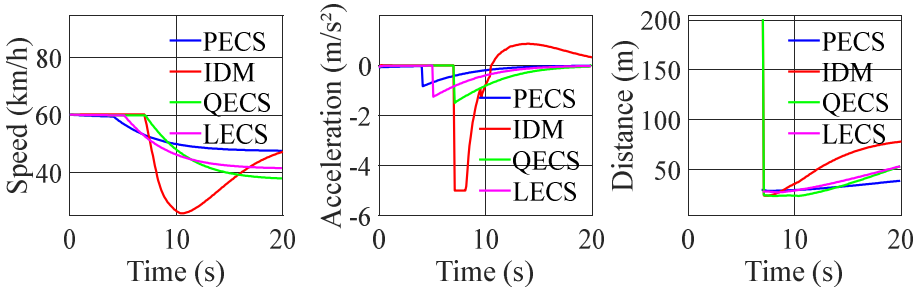
Fig. 16. The results of Case 1.

Table 7 Robustness analysis results for Case 1 under data missingness and Gaussian noise disturbances.

Strategy	Energy consumption (kJ)	Improvement (%)	Cut-in distance (m)
IDM	130.35	-	28.21
PECS with complete data	99.43	23.72	41.58
PECS with 10% miss data	100.45	22.83	41.25
PECS with 20% miss data	102.94	22.51	41.04
PECS with 30% miss data	106.59	20.87	40.62
PECS with Low-level Gaussian noise	100.31	23.04	41.36
PECS with High-level Gaussian noise	101.26	21.31	40.86

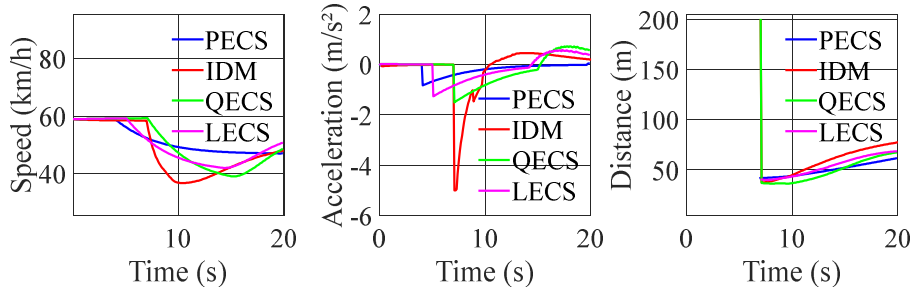
Fig. 17 presents the simulation results for Case 2. Compared with Case 1, this scenario involves higher initial speeds for both the ego vehicle and the cut-in vehicle, and the cut-in vehicle enters the lane at a lower speed than the ego vehicle. Under these conditions, all four strategies exhibit prolonged phases accompanied by more pronounced speed fluctuations with the increase of cut-in speed. Additionally, under the high-speed cut-in scenario,

the proposed method achieves a lower peak deceleration of only -0.83 m/s², indicating a smoother braking response with the increase of cut-in speed. Case 2 represents the most significant potential safety risk among the four cases because the initial speed of the ego vehicle is higher than that of the cut-in vehicle, resulting in the largest relative speed at the cut-in moment. To further evaluate the driving safety, the time-to-collision (TTC) is adopted for safety assessment. The TTC values of IDM and QECS at the cut-in instant are 7.48 s and 7.89 s, respectively, both remaining within a relatively safe range. In contrast, the TTC values of PECS and LECS are infinite, as both strategies proactively adjust driving speed before the cut-in maneuver. These results further demonstrate that the proposed strategy can maintain favorable safety performance in high-risk cut-in scenarios. Fig. 18 illustrates another scenario in which the initial speed of the ego vehicle and the cut-in speed of the target vehicle are similar to those in Case 2, but with a larger cut-in distance. Compared with Case 2, the amplitude of speed fluctuations is reduced for all four strategies, indicating that increasing the cut-in distance alleviates the disturbance intensity imposed on the ego vehicle. Benefiting from accurate prediction of the target vehicle's cut-in trajectory, PECS achieves the smallest variations in both speed and acceleration.



(a) Vehicle speed. (b) Vehicle Acceleration. (c) Intervehicle distance.

Fig. 17. The results of Case 2.

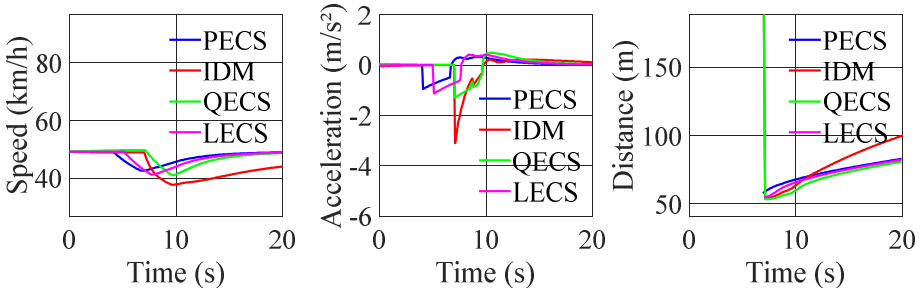


(a) Vehicle speed. (b) Vehicle Acceleration. (c) Intervehicle distance.

Fig. 18. The results of Case 3.

Fig. 19 illustrates the results of Case 4 which corresponds to the scenario with the largest cut-in distance among all the four cases. Except for the IDM, the remaining three strategies maintain a minimum speed around 41 km/h throughout the cut-in procedure. As the cut-in distance increases, all the four strategies exhibit slight performance

differences. The reason is that under conditions of a larger cut-in distance and similar speeds between the ego and cut-in vehicles, the disturbance introduced by the cut-in maneuver is relatively mild, limiting the potential benefits of advanced prediction-based strategies. Although the performance advantage of the PECS is reduced in this scenario, it still achieves the lowest peak deceleration.



(a) Vehicle speed. (b) Vehicle Acceleration. (c) Intervehicle distance.

Fig. 19. The results of Case 4.

All validation results are summarized in Table 8. The PECS achieves the highest energy efficiency in all four cases, reaching the maximum improvement of 41.66% in Case 2, corresponding to a reduction of 104.51 kJ in energy consumption. It therefore significantly outperforms LECS and QECS. It also provides the best travel efficiency, achieving a 16.03% improvement in Case 2. Compared with Case 2, the energy efficiency gain of the PECS declines to 32.54% in Case 3 as the cut-in distance increases. This declining trend is consistent with the pattern illustrated in Fig. 15, indicating that the PECS is particularly effective under closer cut-in distances. Additionally, the PECS consistently confines the max jerk within 6 m/s^3 under different cut-in conditions, demonstrating favorable driving comfort.

Table 8 Performance comparison of the four strategies in different cases.

Strategy	Energy consumption (kJ) / efficiency improvement (%)				Travel efficiency improvement (%)				Max jerk (m/s^3)			
	Case 1	Case 2	Case 3	Case 4	Case 1	Case 2	Case 3	Case 4	Case 1	Case 2	Case 3	Case 4
IDM	130.34/-	250.87/-	213.49/-	178.78/-	-	-	-	-	25.00	25.00	24.99	15.48
QECS	121.99/6.40	196.84/21.54	193.07/9.56	176.61/1.21	6.50	9.95	4.03	8.02	9.87	7.46	7.53	6.48
LECS	113.21/13.14	174.95/30.26	172.27/19.30	169.89/4.97	6.96	9.92	4.12	7.34	8.21	6.25	6.33	5.65
PECS	98.52/23.72	146.36/41.66	144.01/32.54	164.12/8.20	12.67	16.03	7.14	7.97	6.01	4.02	4.07	4.71

To further evaluate the overall effectiveness of the PECS, a weighted composite improvement index is introduced by integrating improvements in both energy efficiency and travel efficiency. In this index, the weighting coefficients for energy efficiency and travel efficiency are set to 0.741 and 0.227, respectively [48]. Table 9 summarizes the comprehensive performance improvements of the four strategies. As shown in the results, the PECS achieves more pronounced performance gains in Cases 2 and 3 compared with the other two cases, reaching 34.50% and 25.73%, respectively. In these two cases, both the ego vehicle and the cut-in vehicle travel at relatively higher

speeds, indicating that PECS delivers better overall performance under more aggressive cut-in scenarios. Overall, simulation results under real-world cut-in scenarios indicate that the PECS effectively reduces energy consumption while maintaining preferable travel efficiency. This advantage stems from its use of spatiotemporal interactions to anticipate lane-change maneuvers, enabling earlier and smoother speed adjustments that minimize energy consumption and enhance overall efficiency.

Table 9 The comprehensive performance comparison.

Strategy	Comprehensive performance improvement (%)			
	Case 1	Case 2	Case 3	Case 4
IDM	-	-	-	-
QECS	6.21	18.21	7.99	2.71
LECS	11.31	24.67	15.23	5.34
PECS	20.45	34.50	25.73	7.88

V. CONCLUSIONS

To address lateral stochastic disturbances from HDVs in mixed traffic scenario, this paper proposes a spatiotemporal predictive eco-cruising strategy for ECAVs. The proposed strategy predicts lane-change trajectories by exploiting spatiotemporal relationship among multiple vehicles and subsequently optimizes ecological velocity of the ego vehicle. A two-layer framework is developed in this strategy, in which the upper layer utilizes a transformer-based model to extract spatiotemporal features and predict the lane-change trajectories of the potential cut-in vehicles. Real-world motion trajectory data are employed to train the prediction model, enabling accurate prediction of the lane-change behaviors. In the lower layer, the predicted trajectories are embedded into a MPC framework, where ecological velocity optimization is solved via QP algorithm. Numerous tests are conducted to validate the effectiveness of the proposed strategy using the NGSIM dataset. The constructed prediction model is verified to accurately anticipate lane-change trajectories under complex spatiotemporal conditions. Moreover, compared with the baseline strategy, the proposed PECS achieves an average energy efficiency improvement of 16.23%, while simultaneously enhancing energy efficiency, driving comfort and travel efficiency.

Future research will focus on validating the proposed strategy through human-in-the-loop experiment and further investigating practical deployment uncertainties, such as delayed perception and communication latency. Meanwhile, the proposed strategy does not account for variations in road geometry and vehicle types. The generalization capability of the proposed strategy under more diverse traffic environments will be further investigated.

ACKNOWLEDGMENTS

The work is funded by the National Natural Science Foundation of China (No. 52502468), Guangxi Natural Science Foundation (No. 2025GXNSFBA069291) in part. Any opinions expressed in this paper are solely those of the authors and do not represent those of the sponsors.

REFERENCES

[1] G. Li, D. Görges, and M. Wang, "Online optimization of gear shift and velocity for eco-driving using adaptive dynamic programming," *IEEE transactions on intelligent vehicles,* vol. 7, no. 1, pp. 123-132, 2021.

[2] J. Cai, Y. Liu, Y. Zhang, S. Shen, Z. Lei, and Z. Chen, "Hierarchical cooperative eco-driving optimization for multidimensional mixed vehicles at signalized intersections," *Energy,* vol. 325, p. 136174, 2025.

[3] Z. Fang, Z. Chen, Q. Yu, B. Zhang, and R. Yang, "Online power management strategy for plug-in hybrid electric vehicles based on deep reinforcement learning and driving cycle reconstruction," *Green Energy and Intelligent Transportation,* vol. 1, no. 2, p. 100016, 2022.

[4] Z. Chen, S. Wu, S. Shen, Y. Liu, F. Guo, and Y. Zhang, "Co-optimization of velocity planning and energy management for autonomous plug-in hybrid electric vehicles in urban driving scenarios," *Energy,* vol. 263, p. 126060, 2023.

[5] J. Liu *et al.*, "Eco-friendly on-ramp merging strategy for connected and automated vehicles in heterogeneous traffic," *IEEE Transactions on Vehicular Technology,* vol. 72, no. 11, pp. 13888-13900, 2023.

[6] Y. Huang, E. C. Ng, J. L. Zhou, N. C. Surawski, E. F. Chan, and G. Hong, "Eco-driving technology for sustainable road transport: A review," *Renewable and sustainable energy reviews,* vol. 93, pp. 596-609, 2018.

[7] L. Guo *et al.*, "Co-optimization strategy of unmanned hybrid electric tracked vehicle combining eco-driving and simultaneous energy management," *Energy,* vol. 246, p. 123309, 2022.

[8] P. Liao, T.-Q. Tang, R. Liu, and H.-J. Huang, "An eco-driving strategy for electric vehicle based on the powertrain," *Applied Energy,* vol. 302, p. 117583, 2021.

[9] S. Wang and X. Lin, "Eco-driving control of connected and automated hybrid vehicles in mixed driving scenarios," *Applied Energy,* vol. 271, p. 115233, 2020.

[10] H. Lee, K. Kim, N. Kim, and S. W. Cha, "Energy efficient speed planning of electric vehicles for car-following scenario using model-based reinforcement learning," *Applied Energy,* vol. 313, p. 118460, 2022.

[11] Y. Wu, Y. Liu, J. Peng, Z. Chen, Y. Liu, and Y. Zhang, "Enhanced Hierarchical Eco-Driving Control for Electric Vehicles via Global Velocity Optimization with Road Slope Adaptation," *IEEE Transactions on Transportation Electrification,* 2025.

[12] S. R. Deshpande, D. Jung, L. Bauer, and M. Canova, "Integrated approximate dynamic programming and equivalent consumption minimization strategy for eco-driving in a connected and automated vehicle," *IEEE Transactions on Vehicular Technology,* vol. 70, no. 11, pp. 11204-11215, 2021.

[13] Z. Lei *et al.*, "Hierarchical eco-driving control for plug-in hybrid electric vehicles under multiple signalized intersection scenarios," *Journal of Cleaner Production,* vol. 420, p. 138420, 2023.

[14] T. Jayson, A. Bakibillah, C. P. Tan, M. Kamal, V. Monn, and J.-i. Imura, "Electric vehicle eco-driving strategy at signalized intersections based on optimal energy consumption," *Journal of Environmental Management,* vol. 368, p. 122245, 2024.

[15] C. Wang, Z. Yang, L. Zhu, and L. Zhang, "Learning-augmented hierarchical control for signal-aware safe eco-driving of connected autonomous vehicles," *Applied Energy,* vol. 401, p. 126807, 2025.

[16] K. Lu, Y. Chen, Y. Tong, J. Zhang, Y. Luo, and J. Wang, "Eco-driving control for CAVs at signalized intersections: Adapting to traffic uncertainties," *Transportation Research Part D: Transport and Environment,* vol. 132, p. 104270, 2024.

[17] Z. Zhu, S. Gupta, A. Gupta, and M. Canova, "A deep reinforcement learning framework for eco-driving in connected and automated hybrid electric vehicles," *IEEE transactions on vehicular technology,* vol. 73, no. 2, pp. 1713-1725, 2023.

[18] Y. Yan *et al.*, "Eco-coasting controller using road grade preview: Evaluation and online implementation

based on mixed integer model predictive control," *IEEE Transactions on Vehicular Technology,* vol. 72, no. 10, pp. 12508-12523, 2023.
[19] A. Hamednia, N. Murgovski, J. Fredriksson, J. Forsman, M. Pourabdollah, and V. Larsson, "Optimal thermal management, charging, and eco-driving of battery electric vehicles," *IEEE Transactions on Vehicular Technology,* vol. 72, no. 6, pp. 7265-7278, 2023.
[20] M. Mirabilio, A. Iovine, E. De Santis, M. D. Di Benedetto, and G. Pola, "A mesoscopic human-inspired adaptive cruise control for eco-driving," *IEEE Transactions on Intelligent Transportation Systems,* vol. 24, no. 9, pp. 9571-9583, 2023.
[21] Y. Zhang, X. Qu, and L. Tong, "Optimal eco-driving control of autonomous and electric trucks in adaptation to highway topography: Energy minimization and battery life extension," *IEEE Transactions on Transportation Electrification,* vol. 8, no. 2, pp. 2149-2163, 2022.
[22] J. Li, X. Wu, J. Fan, Y. Liu, and M. Xu, "Overcoming driving challenges in complex urban traffic: A multi-objective eco-driving strategy via safety model based reinforcement learning," *Energy,* vol. 284, p. 128517, 2023.
[23] T. Ard, L. Guo, J. Han, Y. Jia, A. Vahidi, and D. Karbowski, "Energy-efficient driving in connected corridors via minimum principle control: Vehicle-in-the-loop experimental verification in mixed fleets," *IEEE Transactions on Intelligent Vehicles,* vol. 8, no. 2, pp. 1279-1291, 2023.
[24] J. Li, A. Fotouhi, W. Pan, Y. Liu, Y. Zhang, and Z. Chen, "Deep reinforcement learning-based eco-driving control for connected electric vehicles at signalized intersections considering traffic uncertainties," *Energy,* vol. 279, p. 128139, 2023.
[25] K. Lu, D. Li, Q. Wang, K. Yang, L. Zhao, and Z. Song, "Safe reinforcement learning-based eco-driving control for mixed traffic flows with disturbances," *IEEE Transactions on Intelligent Transportation Systems,* 2025.
[26] B. Li *et al.*, "Traffic-aware ecological cruising control for connected electric vehicle," *IEEE Transactions on Transportation Electrification,* 2023.
[27] Y. Hu *et al.*, "A generic approach to eco-driving of connected automated vehicles in mixed urban traffic and heterogeneous power conditions," *IEEE Transactions on Intelligent Transportation Systems,* vol. 24, no. 11, pp. 11963-11980, 2023.
[28] Y. Hu *et al.*, "Eco-driving of connected autonomous vehicles in urban traffic networks of mixed autonomy with cut-in and escape lane-changes of manually-driven vehicles," *Transportation Research Part C: Emerging Technologies,* vol. 169, p. 104889, 2024.
[29] X. Wang, J. Liu, H. Lin, S. Garg, and M. Alrashoud, "A multi-modal spatial–temporal model for accurate motion forecasting with visual fusion," *Information Fusion,* vol. 102, p. 102046, 2024.
[30] H. Sadid and C. Antoniou, "Dynamic Spatio-temporal Graph Neural Network for Surrounding-aware Trajectory Prediction of Autonomous Vehicles," *IEEE Transactions on Intelligent Vehicles,* 2024.
[31] D. Li *et al.*, "Planning-inspired hierarchical trajectory prediction via lateral-longitudinal decomposition for autonomous driving," *IEEE Transactions on Intelligent Vehicles,* 2023.
[32] G. Chen, Z. Gao, M. Hua, B. Shuai, and Z. Gao, "Lane change trajectory prediction considering driving style uncertainty for autonomous vehicles," *Mechanical Systems and Signal Processing,* vol. 206, p. 110854, 2024.
[33] C. R. He and N. Li, "Eco-driving Accounting for Interactive Cut-in Vehicles," in *2024 IEEE International Conference on Mobility, Operations, Services and Technologies (MOST)*, 2024: IEEE, pp. 90-100.
[34] S. He, S. Wang, Y. Shao, Z. Sun, and M. W. Levin, "A Connectivity-Based Real-Time Traffic Prediction Considering Lane-Changing Maneuvers with Application to Eco-Driving Control of Electric Vehicles," *IEEE Transactions on Vehicular Technology,* 2025.
[35] Y. Liang, H. Dong, D. Li, and Z. Song, "Adaptive eco-cruising control for connected electric vehicles considering a dynamic preceding vehicle," *eTransportation,* vol. 19, p. 100299, 2024.
[36] E. Abolfazli, B. Besselink, and T. Charalambous, "Minimum time headway in platooning systems under the MPF topology for different wireless communication scenario," *IEEE Transactions on Intelligent Transportation Systems,* vol. 24, no. 4, pp. 4377-4390, 2023.
[37] H. Liu *et al.*, "Eco-driving strategy for connected automated vehicles in mixed traffic flow," *Physica A: Statistical Mechanics and its Applications,* vol. 633, p. 129388, 2024.
[38] V. Bharilya and N. Kumar, "Machine learning for autonomous vehicle's trajectory prediction: A

comprehensive survey, challenges, and future research directions," *Vehicular Communications,* p. 100733, 2024.
[39] A. Vaswani *et al.*, "Attention is all you need," *Advances in neural information processing systems,* vol. 30, 2017.
[40] B. Coifman and L. Li, "A critical evaluation of the Next Generation Simulation (NGSIM) vehicle trajectory dataset," *Transportation Research Part B: Methodological,* vol. 105, pp. 362-377, 2017.
[41] Z. Liu *et al.*, "Multi-scale temporal fusion transformer for incomplete vehicle trajectory prediction," *IEEE Transactions on Intelligent Vehicles,* 2024.
[42] C. Chen, X. Chen, C. Guo, and P. Hang, "Trajectory Prediction for Autonomous Driving Based on Structural Informer Method," *IEEE Transactions on Automation Science and Engineering,* 2023.
[43] Q. Wang *et al.*, "Adaptive leading cruise control in mixed traffic considering human behavioral diversity," *IEEE Transactions on Intelligent Transportation Systems,* vol. 25, no. 6, pp. 5059-5070, 2023.
[44] A. Koch, L. Nicoletti, T. Herrmann, and M. Lienkamp, "Implementation and analyses of an eco-driving algorithm for different battery electric powertrain topologies based on a split loss integration approach," *Energies,* vol. 15, no. 15, p. 5396, 2022.
[45] O. Derbel, T. Peter, H. Zebiri, B. Mourllion, and M. Basset, "Modified intelligent driver model for driver safety and traffic stability improvement," *IFAC Proceedings Volumes,* vol. 46, no. 21, pp. 744-749, 2013.
[46] Q. Li, R. Cheng, and H. Ge, "Short-term vehicle speed prediction based on BiLSTM-GRU model considering driver heterogeneity," *Physica A: Statistical Mechanics and its Applications,* vol. 610, p. 128410, 2023.
[47] N. Rezazadeh, M. A. Amirabadi, and M. H. Kahaei, "Deep learning-based location prediction in VANET," *IET Intelligent Transport Systems,* vol. 18, no. 9, pp. 1574-1587, 2024.
[48] J. Li, Y. Liu, J. Cheng, A. Fotouhi, and Z. Chen, "Eco-Driving Control for Connected Plug-in Hybrid Electric Vehicles in Urban Scenarios with Enhanced Lane Change Engagement," *Energy,* p. 133294, 2024.

DSPACE

https://dspace.org/

Eco-cruising control under cut-in maneuvers using spatiotemporal attention-based trajectory prediction

Li, Jie; Li, Shengrong; Lan, Yuhang; Fotouhi, Abbas; Liu, Yonggang ...

2026-09-30
Elsevier
https://doi.org/10.1016/j.energy.2026.141560
Li J, Li S, Lan Y, et al., (2026) Eco-cruising control under cut-in maneuvers using spatiotemporal attention-based trajectory prediction. Energy, Volume 360, September 2026, Article number 141560

Downloaded from a DSpace repository. https://dspace.org/